GERMAN - MONGOLIAN INSTITUTE
FOR RESOURCES AND TECHNOLOGY

The present work was submitted to

the German-Mongolian Institute for Resource and Technology

Predictive Maintenance of Electric Motor-System Using Vibration Analysis

Bachelor Thesis

by

Tuvshinbayar Boldbaatar

Study Program: Mechanical Engineering

Student ID: B2200579

Supervisor 1 / Examiner 1 **Prof. Sungchil Lee**

Supervisor 2 / Examiner 2 **Prof. Young Suk Kim**

Ulaanbaatar/Nalaikh,

1st of May, 2026

Statutory Declaration

Boldbaatar, Tuvshinbayar	B2200579
Last Name, First Name	Student ID Number

I hereby affirm in lieu of an oath that I provided the submitted bachelor thesis

Predictive Maintenance of Electric Motor-System Using Vibration Analysis

I did not use any sources other than those stated. In case that the work is additionally submitted on a data medium, I declare that the written and the electronic form are completely identical. The work was not submitted in the same or similar form to any examination authority.

Ulaanbaatar, Mongolia May, 1,2026	ТуВшинБаяр
Place, Date	Signature

Acknowledgement

First of all, I am thanking my university The German-Mongolian Institute for Resources and Technology, and all the professors, and lecturers for giving me the knowledge over the past five years.

I would like to express my deepest appreciation to my supervisors, Prof. Sungchil Lee and Prof. Young Suk Kim**,** for their continuous support, valuable guidance, and insightful feedback throughout this study. Their advice helped me understand the importance of approaching engineering problems with critical thinking and conducting research in a thorough and systematic manner, without overlooking important details. Their mentorship played a significant role in improving both the quality of this work and my understanding of the subject.

I am also grateful to my friends and classmates for their encouragement and support during my studies.

Finally, I would like to express my heartfelt thanks to my family for their constant support, patience, and motivation throughout my academic journey.

Many thanks,

Tuvshinbayar Boldbaatar

Abstract

Electric motors are widely used in industrial and mining operations, where their reliability directly affects productivity, safety, and maintenance costs. Unexpected failures can lead to significant downtime, making predictive maintenance an important strategy for improving system performance. This study investigates the use of vibration analysis to detect common mechanical faults in electric motors, including bearing defects, misalignment, and unbalance. Publicly available datasets, including the Case Western Reserve University (CWRU) bearing dataset and a belt-driven rotating shaft system dataset from the Mendeley Data repository, are used to analyze vibration signals under both normal and faulty conditions. For bearing fault detection, signals from healthy and defective cases are compared using time-domain, frequency-domain, and envelope analysis, allowing both general vibration behavior and high-frequency impacts to be examined. The data are sampled at 12 kHz, with the motor operating at 1797 rpm, enabling identification of localized inner race defects. In addition, vibration data from a belt-driven rotating shaft system are used to study unbalance and misalignment. Normal operation is compared separately with each fault condition using time-domain and frequency-domain methods. The shaft operates at 1238 rpm, and Fast Fourier Transform (FFT) analysis focuses on the shaft rotational frequency (1X) and its harmonics (2X and 3X) for fault identification. The results show that different fault types produce distinct vibration patterns, though the clarity of detection depends on sensor placement and measurement direction, allowing clear fault differentiation. A combination of time-domain features, harmonic analysis, and envelope methods provides a more reliable diagnosis than using a single parameter. Overall, this study demonstrates that vibration analysis can effectively detect both motor-related and externally induced faults, supporting early fault detection and improving predictive maintenance strategies.

Contents

Statutory Declaration 2
Acknowledgement 3
Abstract 4
List of Figures 7
List of Tables 9
List of Abbreviation 10
Chapter 1 Introduction 11
1.1 Background 11
1.2 Problem Statement 12
1.3 Objective 13
Chapter 2 Literature Review 14
2.1 Introduction to Vibration Analysis 14
2.2 Vibration Signal Analysis Method 14
2.2.1 Time Domain Analysis 15
2.2.2 Frequency Domain Analysis 16
2.2.3 Envelope Analysis 17
2.2.4 Signal Tracking in Vibration Analysis 18
2.3 Common Mechanical Faults in Rotating Systems 19
2.3.1 Unbalance 19
2.3.2 Misalignment 20
2.3.3 Bearing Fault 21
2.4 Structural Resonance 22
2.5 Additional & Non-Fault Vibrations 22
Chapter 3 Abnormal State Detecting Methodology 23
3.1 Research Design 23
3.2 Data Description 23
3.2.1 Bearing Fault Dataset 23
3.2.2 Belt-Driven System Dataset 24
3.3 Signal Preprocessing & Analysis 25
3.3.1 Time Domain Analysis 26
3.3.2 Frequency Domain Analysis 26
3.3.3 Envelope Analysis 27
3.4 Signal Tracking & Fault Identification 27
Chapter 4 Result & Discussion 28
4.1 Bearing Fault & Normal Condition 28
4.1.1 Time Domain Analysis 28

4.1.2 Frequency Domain Analysis 30
4.1.3 Envelope Analysis 31
4.1.4 Discussion 32
4.2 Unbalance & Normal Condition 32
4.2.1 Time Domain & Frequency Domain Analysis 33
4.2.2 Discussion 38
4.3 Misalignment & Normal Condition 39
4.3.1 Time Domain & Frequency Domain Analysis 40
4.3.2 Discussion 45
Chapter 5 Conclusion 46
5.1 Summary of Findings 46
5.2 Key Insights 47
5.2.1 System Behavior 47
5.2.2 Sensor Placement 47
5.2.3 Practical Understanding 47
5.3 Limitations & Future work 48
Reference 49
Appendixes 51
Appendix 1 Conversion 51
Appendix 2 51
Appendix 2.1 Misalignment & Normal Condition 51
Appendix 2.2 Unbalance & Normal Condition 53
Appendix 3 Bearing Fault & Normal Condition 55

List of Figures

FIGURE 1 INTERNAL STRUCTURE OF AN ELECTRIC MOTOR 7

FIGURE 2 DISTRIBUTION OF ELECTRIC MOTOR FAILURES BASED ON IEEE AND EPRI 11

FIGURE 3 ILLUSTRATION OF ROTOR UNBALANCE SHOWING CENTRIFUGAL FORCE 19

FIGURE 4 PARALLEL MISALIGNMENT AND ITS VIBRATION CHARACTERISTICS 20

FIGURE 5 ANGULAR MISALIGNMENT AND ITS VIBRATION CHARACTERISTICS 20

FIGURE 6 COMPARISON OF PARALLEL AND ANGULAR MISALIGNMENT WITH FREQUENCY COMPONENTS 21

FIGURE 7 ROLLING ELEMENT BEARING COMPONENTS AND STRUCTURE 21

FIGURE 8 TEST BENCH (CASE WESTERN RESERVE UNIVERSITY) 23

FIGURE 9 TEST BENCH (MENDELEY REPOSITORY) 25

FIGURE 10 TIME-DOMAIN COMPARISON OF NORMAL AND BEARING FAULT CONDITIONS 28

FIGURE 11 FREQUENCY-DOMAIN (FFT) COMPARISON OF NORMAL AND BEARING FAULT CONDITIONS 30

FIGURE 12 ENVELOPE SPECTRUM SHOWING CHARACTERISTIC BEARING FAULT FREQUENCIES 31

FIGURE 13 TIME AND FREQUENCY-DOMAIN COMPARISON OF NORMAL AND UNBALANCE CONDITION (SENSOR 1) 33

FIGURE 14 TIME AND FREQUENCY-DOMAIN COMPARISON OF NORMAL AND UNBALANCE CONDITION (SENSOR 2) 34

FIGURE 15 TIME AND FREQUENCY-DOMAIN COMPARISON OF NORMAL AND UNBALANCE CONDITION (SENSOR 3) 36

FIGURE 16 TIME AND FREQUENCY-DOMAIN COMPARISON OF NORMAL AND UNBALANCE CONDITION (SENSOR 4) 37

FIGURE 17 TIME AND FREQUENCY-DOMAIN COMPARISON OF NORMAL AND MISALIGNMENT CONDITION (SENSOR 1) 40

FIGURE 18 TIME AND FREQUENCY-DOMAIN COMPARISON OF NORMAL AND MISALIGNMENT CONDITION (SENSOR 2)..... 41

FIGURE 19 TIME AND FREQUENCY-DOMAIN COMPARISON OF NORMAL AND MISALIGNMENT CONDITION (SENSOR 3)..... 43

FIGURE 20 TIME AND FREQUENCY-DOMAIN COMPARISON OF NORMAL AND MISALIGNMENT CONDITION (SENSOR 4)..... 44

List of Tables

TABLE 1 STATISTICAL FEATURE COMPARISON BETWEEN NORMAL AND BEARING FAULT CONDITIONS 29

TABLE 2 STATISTICAL FEATURE COMPARISON BETWEEN NORMAL AND UNBALANCE CONDITION FOR SENSOR 1 33

TABLE 3 STATISTICAL FEATURE COMPARISON BETWEEN NORMAL AND UNBALANCE CONDITION (SENSOR 2) 35

TABLE 4 STATISTICAL FEATURE COMPARISON BETWEEN NORMAL AND UNBALANCE CONDITION FOR SENSOR 3 36

TABLE 5 STATISTICAL FEATURE COMPARISON BETWEEN NORMAL AND UNBALANCE CONDITION FOR SENSOR 4 37

TABLE 6 SUMMARY OF STATISTICAL FEATURE CHANGES FOR UNBALANCE ACROSS ALL SENSORS 39

TABLE 7 STATISTICAL FEATURE COMPARISON BETWEEN NORMAL AND MISALIGNMENT CONDITION FOR SENSOR 1 40

TABLE 8 STATISTICAL FEATURE COMPARISON BETWEEN NORMAL AND MISALIGNMENT CONDITION FOR SENSOR 2 42

TABLE 9 STATISTICAL FEATURE COMPARISON BETWEEN NORMAL AND MISALIGNMENT CONDITION FOR SENSOR 3 43

TABLE 10 STATISTICAL FEATURE COMPARISON BETWEEN NORMAL AND MISALIGNMENT CONDITION FOR SENSOR 4 44

TABLE 11 SUMMARY OF STATISTICAL FEATURE CHANGES FOR MISALIGNMENT ACROSS ALL SENSORS 46

List of Abbreviation

FFT	Fast Fourier Transform
RMS	Root Mean Square
BPFI	Ball Pass Frequency Inner Race
BPFO	Ball Pass Frequency Outer Race
BSF	Ball Spin Frequency
FTF	Fundamental Train Frequency
CWRU	Case Western Reserve University
EDM	Electro-Discharge Machining
DE	Drive End
FE	Fan End
RPM	Revolutions Per Minute
Hz	Hertz
1X	Shaft rotational frequency
2X	Second harmonic of shaft rotational frequency
3X	Third harmonic of shaft rotational frequency
mat	MATLAB data file format
npy	NumPy array file format

Chapter 1 Introduction

1.1 Background

Electric motors are essential components in industrial and mining systems, where they provide continuous mechanical power for critical operations. Their reliability directly influences productivity, operational safety, and maintenance costs [1]. In such environments, even minor mechanical faults can develop into serious failures if not detected early, leading to unplanned downtime and economic loss [3].

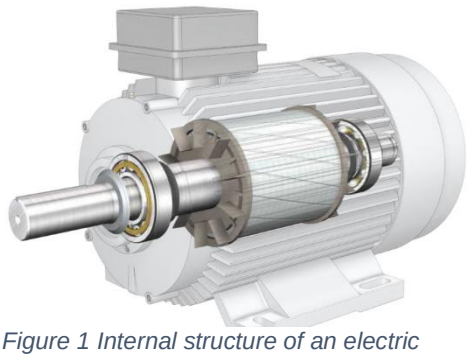


Figure 1 Internal structure of an electric motor [10]

Figure 1 shows the internal structure of an electric motor, including key components such as the rotor, shaft, and bearings. These parts work together to convert electrical energy into mechanical motion. Among them, the rotating elements, especially the shaft and bearings, are more vulnerable to mechanical damage because they operate under continuous dynamic stress. For this reason, faults in these components are among the most critical issues affecting motor performance.

In general, all rotating machines generate vibration during normal operation. While this is not inherently problematic, any deviation from the normal vibration pattern can indicate the presence of mechanical faults. Changes in vibration amplitude, frequency content, or signal behavior are commonly associated with faults such as unbalance, misalignment, and bearing damage. For this reason, vibration analysis has become a widely used tool for condition monitoring and predictive maintenance.

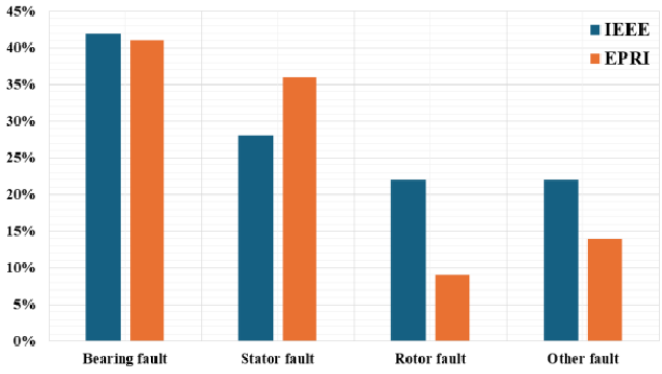


Figure 2 Distribution of electric motor failures based on IEEE and EPRI [11]

Figure 2 presents the distribution of common electric motor faults based on studies conducted by IEEE and EPRI. It can be clearly seen that bearing faults are the most frequent, accounting for approximately 40–45% of all failures, while stator and

rotor faults occur less often. This highlights the importance of focusing on bearing-related issues when analyzing vibration signals and diagnosing machine conditions. The strength of vibration analysis lies in its ability to describe machine behavior through measurable signal characteristics [1]. In particular, frequency-domain analysis is widely used to identify faults based on their characteristic frequencies. To better understand these changes, vibration signals are often analyzed in the frequency domain, where different fault types produce characteristic frequency patterns. For example, unbalance is typically associated with vibration at the rotational frequency (1×), while misalignment often introduces additional harmonics such as 2× and 3× components [4]. These frequency patterns provide important information about both the type and severity of mechanical faults.

In practical applications, many motor systems operate in belt-driven configurations, where vibration is transmitted through intermediate components such as pulleys and shafts. These components can modify the vibration signal by amplifying or attenuating certain frequency components, making fault identification more complex [4].

Despite the effectiveness of vibration analysis in identifying mechanical faults, its application in belt-driven systems remains challenging. As discussed, vibration signals in such systems are influenced not only by the fault itself but also by the transmission path and structural dynamics of interconnected components [7]. Consequently, the measured signal may not directly represent the original fault characteristics, making interpretation more complex. This limitation highlights the need for a more systematic analysis approach that considers both signal behavior and system dynamics.

1.2 Problem Statement

Although vibration analysis is widely used for fault detection in rotating machinery, accurate fault identification in real systems remains challenging. In belt-driven systems, vibration signals do not originate from a single component but propagate through interconnected elements such as shafts, pulleys, and belts. As a result, the measured vibration signal is a combination of multiple dynamic effects rather than a direct representation of the fault source.

This complexity makes it difficult to clearly distinguish between different fault types, especially when their vibration characteristics overlap. For example, unbalance and misalignment are typically associated with low-frequency components, while bearing faults generate high-frequency impulsive signals. In addition, sensor placement and

measurement direction significantly influence the observed vibration response, which may lead to incomplete or misleading interpretations. Therefore, a systematic analysis approach is required to accurately interpret vibration signals by considering both signal characteristics and system dynamics. This is essential for improving the reliability of fault detection in practical belt-driven motor systems.

1.3 Objective

The main objective of this study is to investigate how vibration analysis can be used to detect mechanical faults in electric motor systems and to understand how these faults influence system behavior and motor performance.

To achieve this objective, the study aims to:

1. Identify characteristic vibration features associated with different fault types
2. Analyze vibration behavior using time-domain, frequency-domain, and envelope analysis methods
3. Evaluate how sensor placement and measurement direction influence fault detection
4. Examine how vibration propagates through a belt-driven system
5. Assess the impact of mechanical faults on overall motor performance

This study contributes to the understanding of vibration-based fault diagnosis by combining analysis of motor-related bearing faults and shaft-related mechanical faults within a belt-driven system. It highlights how system dynamics and sensor placement influence vibration measurements and fault detectability. The findings provide practical insights for improving predictive maintenance strategies in real industrial applications.

Chapter 2 Literature Review

2.1 Introduction to Vibration Analysis

Vibration analysis is one of the most widely used techniques for condition monitoring and predictive maintenance of rotating machinery. It is based on the principle that every mechanical system produces a characteristic vibration pattern during operation, and any deviation from normal conditions results in measurable changes in this behavior. Vibration can be defined as the oscillatory motion of a mechanical system about its equilibrium position. In rotating machinery, vibration is mainly caused by dynamic forces such as mass imbalance, misalignment, and interactions between mechanical components. These forces generate vibration signals that contain important information about the condition of the system [1].

In practical applications, vibration signals are measured using sensors such as accelerometers, which are typically mounted on machine components like bearings or housings. The measured signals are then analyzed to detect abnormalities and identify potential faults. One of the main advantages of vibration analysis is its ability to detect faults at an early stage, before they lead to serious damage or system failure [3].

Because of its effectiveness and reliability, vibration analysis has become a key tool in modern predictive maintenance strategies. It allows engineers to monitor machine condition continuously and make informed decisions about maintenance and operation.

2.2 Vibration Signal Analysis Method

Vibration signals provide important information about the condition of mechanical systems, but raw data is often complex and difficult to interpret. Therefore, signal analysis methods are used to extract meaningful features and identify fault-related characteristics. In vibration-based condition monitoring, analysis is commonly performed using time-domain, frequency-domain, envelope analysis, and signal tracking techniques. Each method highlights different aspects of the vibration signal and is suitable for detecting specific types of faults. By combining these methods, a more reliable and comprehensive evaluation of machine condition can be achieved [2].

2.2.1 Time Domain Analysis

Time-domain analysis is one of the most fundamental approaches in vibration signal analysis, where the vibration signal is examined as a function of time. In this method, the signal is represented as $x(t)$, showing how the vibration amplitude changes over time. It provides direct insight into the overall behavior of the machine and is particularly useful for detecting general changes in operating conditions. By observing the time-domain signal, it is possible to identify characteristics such as sudden peaks, irregular patterns, or variations in amplitude. These features may indicate abnormal machine behavior, such as impacts, looseness, or early-stage faults. However, visual inspection alone is often not sufficient, and therefore statistical parameters are used to quantify the signal and provide more reliable indicators of machine condition.[7]

- One of the most commonly used parameters is the **Root Mean Square (RMS)** value, which represents the overall energy of the vibration signal:

$$\boldsymbol{RMS} = \sqrt{\frac{\mathbf{1}}{\boldsymbol{N}}\sum_{\boldsymbol{i=1}}^{\boldsymbol{N}} \boldsymbol{x_i^2}}$$

  The RMS value reflects the average vibration level of the system and is widely used as a general indicator of machine health. An increase in RMS typically suggests an increase in vibration energy, which may be associated with developing faults [7].

- Another important parameter is the **Peak Value**, defined as the maximum amplitude of the signal:

$$\boldsymbol{Peak} = \mathbf{max}\,(|\boldsymbol{x_i}|)$$

  The peak value is highly sensitive to sudden impacts or transient events and is useful for detecting faults that produce short-duration high-amplitude signals [7].

- The **Crest Factor**, which is the ratio of the peak value to the RMS value, provides additional information about the nature of the vibration:

$$\boldsymbol{Crest\ Factor} = \frac{\boldsymbol{Peak}}{\boldsymbol{RMS}}$$

A high crest factor indicates the presence of sharp peaks in the signal, which are often associated with impulsive faults such as bearing defects or surface damage [2].

- In addition, **Kurtosis** is a statistical measure that describes the distribution shape of the signal and is particularly sensitive to impulsive behavior:

$$\boldsymbol{Kurtosis} = \frac{\mathbf{1}}{\boldsymbol{N}}\sum_{\boldsymbol{i=1}}^{\boldsymbol{N}}(\frac{\boldsymbol{x_i} - \boldsymbol{\mu}}{\boldsymbol{\sigma}})^{\mathbf{4}}$$

A higher kurtosis value indicates the presence of sharp, high-amplitude peaks in the signal. This makes it especially useful for detecting early-stage bearing faults, where impacts may not significantly affect overall vibration energy but still produce distinct spikes [7].

- Another useful parameter is **Variance**, which measures the spread of the signal around its mean value:

$$\boldsymbol{\sigma^2} = \frac{\mathbf{1}}{\boldsymbol{N}}\sum_{\boldsymbol{i=1}}^{\boldsymbol{N}}(\boldsymbol{x_i} - \boldsymbol{\mu})^{\mathbf{2}}$$

Variance reflects the stability of the vibration signal. Higher variance indicates greater fluctuation in amplitude, which may suggest unstable or irregular machine behavior [2].

Overall, time-domain analysis provides valuable information about the general condition of a machine and is effective for detecting changes in vibration level and impulsive events. However, it does not provide detailed information about the frequency content of the signal. For this reason, it is commonly combined with frequency-domain analysis to achieve more accurate and reliable fault diagnosis [3].

2.2.2 Frequency Domain Analysis

Frequency-domain analysis is a fundamental technique in vibration analysis that focuses on identifying the frequency components present in a vibration signal. The transformation from time domain to frequency domain is performed using the Fourier Transform, which converts a time-based signal into its frequency representation [5].

The Fourier Transform is defined as:

$$\boldsymbol{X(f) = \int_{-\infty}^{\infty} x(t) e^{\{-j2\pi ft\}dt}}$$

This equation describes how the time-domain signal x(t)x(t)x(t) is decomposed into its frequency components. In practical applications, the Fast Fourier Transform (FFT) is used to compute this transformation efficiently for discrete signals [15].

In rotating machinery, vibration signals are closely related to the rotational speed of the shaft. The fundamental frequency, known as the shaft rotational frequency (1X), is calculated as:

$$f_{shaft}(1X) = \frac{RPM}{60}$$

Higher multiples of this frequency are referred to as harmonics:

- 1X = fundamental frequency
- 2X = second harmonic
- 3X = third harmonic

These harmonic components are important indicators of mechanical faults. For example, unbalance typically produces a dominant peak at 1X, while misalignment often introduces additional harmonics such as 2X and 3X [7].

2.2.3 Envelope Analysis

Envelope analysis is used to detect bearing faults by focusing on high-frequency vibration components generated by localized defects. Unlike unbalance or misalignment, which mainly affect low-frequency regions, bearing damage produces repeated impact signals when rolling elements pass over a defect. These impacts are modulated by the shaft rotation and are often not clearly visible in the standard frequency spectrum. Envelope analysis demodulates the high-frequency signal to extract this repeating impact pattern, making fault-related features easier to identify [2].

In this study, envelope analysis is applied to identify characteristic defect frequencies associated with bearing faults. These include:

- Ball Pass Frequency of Inner Race (BPFI)
- Ball Pass Frequency of Outer Race (BPFO)
- Ball Spin Frequency (BSF)
- Fundamental Train Frequency (FTF)

Each type of defect produces peaks at its corresponding characteristic frequency and its harmonics. For example, an inner race defect typically generates peaks at the BPFI frequency. The actual values of these frequencies depend on the shaft rotational speed and the bearing geometry. In this study, the defect frequencies are expressed as multiples of the shaft speed, allowing them to be directly identified in the envelope spectrum [7].

The presence of clear peaks at these characteristic frequencies indicates the existence of localized bearing damage. Therefore, envelope analysis provides an effective tool for detecting early-stage bearing faults that may not be clearly observable using standard time-domain or frequency-domain methods.

2.2.4 Signal Tracking in Vibration Analysis

Signal tracking in vibration analysis refers to the process of monitoring changes in vibration characteristics over time. Instead of analyzing a single vibration signal, this method focuses on observing trends in parameters such as RMS, peak value, or specific frequency components to detect gradual changes in machine condition. In rotating machinery, many faults develop progressively rather than suddenly. By continuously tracking vibration features, it is possible to identify early signs of degradation before they lead to serious damage. For example, a gradual increase in overall vibration level or a steady rise in the amplitude of a specific frequency component may indicate the development of faults such as unbalance, misalignment, or bearing wear.

Signal tracking is widely used in predictive maintenance systems, where vibration data is recorded and analyzed over time. This approach allows engineers to evaluate machine health, predict potential failures, and schedule maintenance more effectively. As a result, signal tracking plays an important role in improving reliability and reducing unexpected downtime in industrial applications [3].

2.3 Common Mechanical Faults in Rotating Systems

Rotating machinery is affected by various mechanical faults that influence its performance and vibration behavior. Among these, unbalance, misalignment, and bearing defects are the most common in industrial applications. Each fault produces characteristic vibration patterns that can be identified through vibration analysis. Understanding these fault mechanisms is essential for accurate condition monitoring and fault diagnosis [4].

2.3.1 Unbalance

Unbalance is one of the most common mechanical faults in rotating machinery and occurs when the mass of a rotating component is not evenly distributed around its axis of rotation [4]. This uneven mass distribution generates a centrifugal force during rotation, which results in periodic vibration.

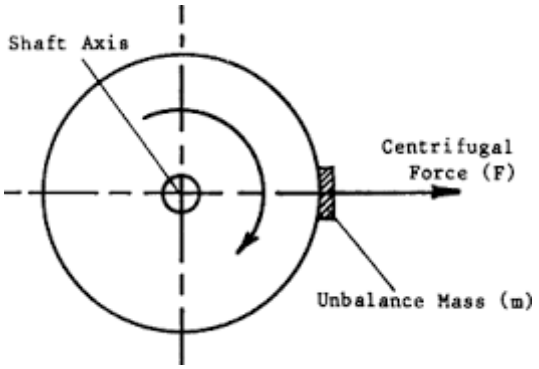


Figure 3 Illustration of rotor unbalance showing centrifugal force [12]

As illustrated in *Figure 3,* the presence of an unbalanced mass creates a rotating centrifugal force that acts outward from the shaft center. This force varies with rotational speed and produces a continuous excitation during operation. The vibration caused by unbalance is typically characterized by a strong peak at the shaft rotational frequency, known as the 1X component. This occurs because the unbalanced mass produces one dominant force per revolution. As the rotational speed increases, the magnitude of this force and the resulting vibration amplitude also increase.

Unbalance generally produces a steady and consistent vibration pattern, mainly in the radial direction. It is usually easier to detect compared to other faults because of its clear frequency signature. However, if not corrected, unbalance can lead to increased stress on bearings and other components, reducing machine life and efficiency [1].

2.3.2 Misalignment

Misalignment is a common mechanical fault that occurs when two connected shafts are not aligned along the same axis. This condition can arise due to improper installation, thermal expansion, or mechanical deformation during operation [4]. Misalignment is generally classified into two main types: parallel misalignment and angular misalignment.

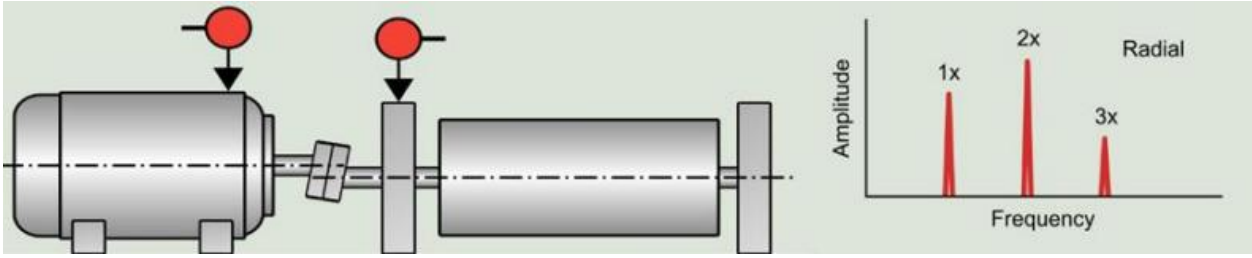


Figure 4 Parallel misalignment and its vibration characteristics [8]

As shown in *Figure 4,* parallel misalignment occurs when the shafts are offset but remain parallel to each other. In this case, vibration is mainly observed in the radial direction [4]. The corresponding frequency spectrum typically shows a dominant peak at the shaft rotational frequency (1X) along with noticeable harmonic components such as 2X and 3X [15].

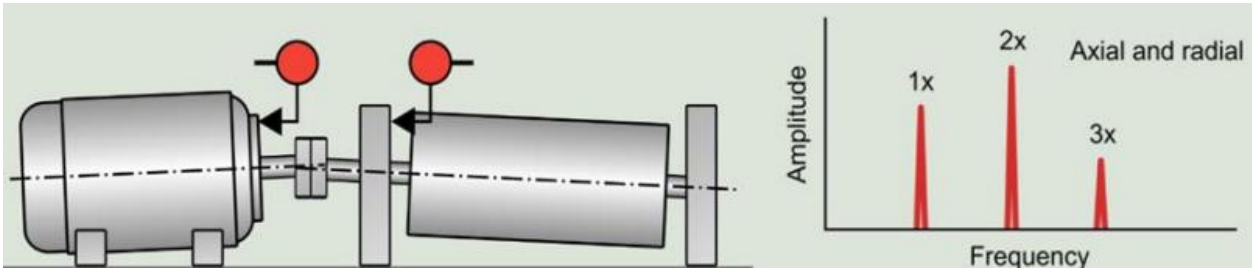


Figure 5 Angular misalignment and its vibration characteristics [8]

In contrast, angular misalignment, illustrated in *Figure 5*, occurs when the shafts are connected at an angle rather than along a straight line. This type of misalignment generates vibration in both axial and radial directions. The frequency spectrum also exhibits strong harmonic components, particularly at 2X, which is commonly considered a key indicator of misalignment [13].

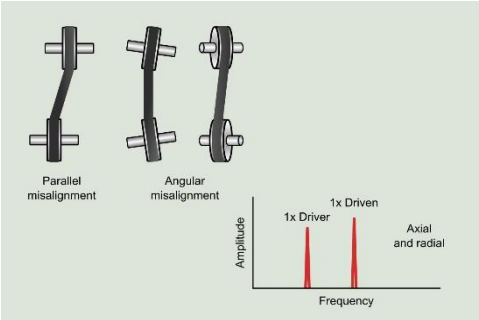


Figure 6 Comparison of parallel and angular misalignment with frequency components [8]

A comparison of these misalignment types is presented in *Figure 6*, where both geometric configurations and their corresponding frequency characteristics are shown. In general, misalignment produces more complex vibration patterns than unbalance due to the presence of multiple excitation forces during each rotation. If not corrected, misalignment can lead to increased stress on couplings, bearings, and shafts, resulting in excessive wear, energy loss, and reduced machine life. Therefore, accurate detection of misalignment through vibration analysis is essential for maintaining system reliability and performance [4].

2.3.3 Bearing Fault

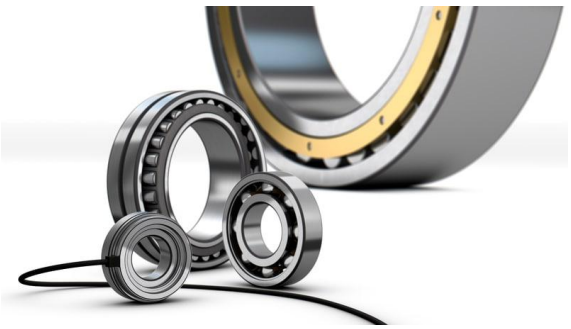


Figure 7 Rolling element bearing components and structure [14]

Rolling element bearings are essential components in rotating machinery, allowing smooth rotation and supporting the shaft. A typical bearing consists of an inner race, outer race, rolling elements, and a cage, as shown in *Figure 7.*

Bearing faults usually occur as localized defects on these components due to wear or fatigue. When a defect is present, repeated impacts are generated as the rolling elements pass over the damaged area. These impacts produce high-frequency vibration signals, which are different from the low-frequency vibrations associated with faults such as unbalance or misalignment. Because these impact signals are often weak and masked by other vibrations, they are not always clearly visible in standard time-domain or frequency-domain analysis. Therefore, techniques such as envelope analysis are used to extract these features and identify characteristic fault frequencies. Bearing faults are critical because they can lead to severe damage if not detected early, making them one of the most important targets in vibration-based condition monitoring [7].

.

2.4 Structural Resonance

Structural resonance occurs when the excitation frequency of a system matches its natural frequency, resulting in a significant increase in vibration amplitude [5]. This condition can occur even in the absence of mechanical faults and is mainly related to the physical properties of the system, such as mass, stiffness, and damping. In rotating machinery, excitation forces may come from normal operation, such as shaft rotation or transmitted forces from connected components. When these forces coincide with the natural frequency of the structure, resonance is triggered, leading to amplified vibration levels. This amplified response often appears as sharp peaks in the frequency spectrum and can be mistaken for fault-related vibration.

Resonance can occur at different frequency ranges depending on the system configuration. In belt-driven systems, structural flexibility and damping effects can shift or amplify certain frequency components, especially in higher frequency regions. As a result, some vibration peaks observed in the frequency spectrum may be related to resonance rather than actual mechanical faults. Understanding resonance is important for accurate fault diagnosis. It helps distinguish between fault-induced vibration and vibration caused by structural behavior, reducing the risk of misinterpretation. Therefore, resonance analysis plays a key role in vibration-based condition monitoring and system evaluation [6].

2.5 Additional & Non-Fault Vibrations

Not all vibration signals are caused by mechanical faults. In rotating systems, especially belt-driven systems, components such as belts and pulleys can modify vibration due to their flexibility and damping properties. This can reduce high-frequency vibrations while allowing low-frequency components to pass through.

In addition, external factors such as structural looseness, motor electrical effects, and environmental disturbances can introduce extra vibration components. These effects may appear in the vibration signal and can be mistaken for faults. Therefore, it is important to distinguish between fault-related and non-fault vibrations to ensure accurate diagnosis and reliable condition monitoring [7].

Chapter 3 Abnormal State Detecting Methodology

3.1 Research Design

This study uses a comparative signal-based analysis method [3] to investigate mechanical faults in electric motors. Vibration signals under different fault conditions are analyzed using publicly available datasets collected by previous researchers. In this approach, vibration signals from different operating conditions are directly compared to identify differences and similarities in their behavior, allowing faults to be recognized based on changes in the signal. The analysis focuses on comparing signals obtained under normal condition, unbalance, misalignment, and bearing fault, in terms of amplitude, frequency content, and signal shape. The main goal is to identify the key characteristics of each fault by comparing these signals. To achieve this, time-domain analysis, frequency-domain analysis using Fast Fourier Transform (FFT), and envelope analysis are applied to study changes in amplitude, frequency components, and impulsive behavior of the signals. The overall research process includes data collection, data preprocessing, signal analysis, and discussion of results.

3.2 Data Description

This section describes the vibration datasets used in this study and their key characteristics. Two publicly available datasets were selected to analyze vibration signals under different fault conditions. These datasets include bearing fault and normal condition data from Case Western Reserve University (CWRU) Bearing Dataset [12], and unbalance, misalignment, and normal condition data from a belt-driven system dataset available in the Mendeley repository [13].

3.2.1 Bearing Fault Dataset

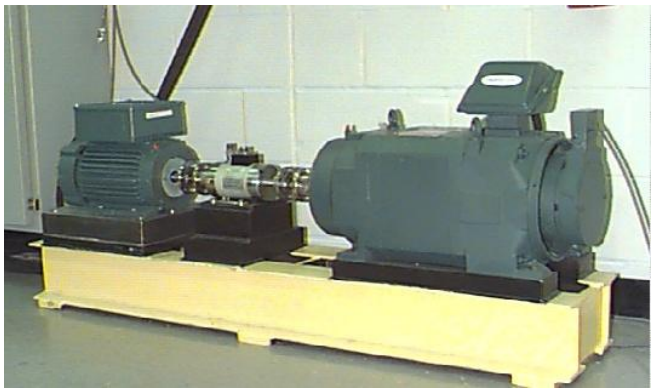


Figure 8 Test Bench (Case Western Reserve University) [12]

Vibration data for bearing fault analysis were obtained from the Case Western Reserve University Bearing Dataset (CWRU) [12]. The dataset includes measurements under both normal and faulty operating conditions, with particular focus on inner race defects. Motor bearings were seeded with faults

using electro-discharge machining (EDM).

For this study, vibration signals corresponding to **normal operating conditions** and **inner race faults with a defect size of 0.007 inches** were selected for analysis. This selection allows a clear comparison between healthy and faulty bearing behavior, while also representing an early-stage defect condition suitable for fault detection analysis. Vibration data were collected using accelerometers mounted on the motor housing with magnetic bases, positioned at the 12 o'clock location at both the drive end and fan end. The bearing used in the experiment is a deep groove ball bearing (SKF 6205-2RS JEM). Its geometrical properties are as follows:

Inner Diameter	Outer Diameter	Ball Diameter	Pitch Diameter
0.9843 inches	2.0472 inches	0.3126 inches	1.537 inches

Based on these parameters, the defect frequencies (multiples of running speed in Hz) are:

Inner Ring (BPFI)	Outer Ring (BPFO)	Cage Train (FTF)	Rolling Element(BSF)
5.4152	3.5848	0.39828	2.3576

These defect frequencies correspond to specific fault locations within the bearing, such as the inner race, outer race, rolling elements, and cage, and serve as important reference values for identifying fault-related components in vibration signals. The vibration signals were sampled at a frequency of 12 kHz, and the motor operated at 1797 rpm (approximately 29.95 Hz), providing the necessary reference for identifying defect-related frequency components in both frequency-domain and envelope analysis.

3.2.2 Belt-Driven System Dataset

Vibration data for analyzing mechanical faults such as unbalance and misalignment were obtained from the Mendeley Data repository [13]. The dataset was developed using a belt-driven rotating system that simulates realistic operating conditions, where different faults were intentionally created to obtain vibration data for various fault types. The test bench consists of an electric motor, frequency inverter, pulleys, belt, rotor (disc), and

bearings, and includes operating conditions such as normal condition, unbalance, misalignment, and mechanical looseness.

A total of 20 tests were conducted, with five tests for each operating condition, including normal condition, unbalance, misalignment, and mechanical looseness. However, the mechanical looseness condition was excluded from the analysis, as it falls outside the scope of this study and typically produces irregular vibration patterns that require a different analytical approach.

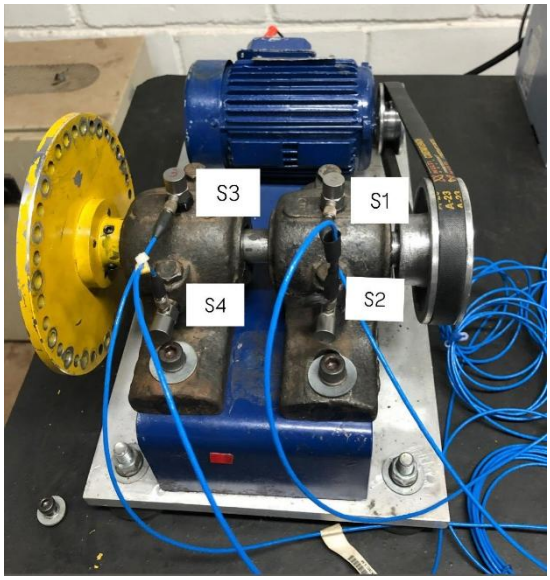


Figure 9 Test Bench (Mendeley Repository) [13]

Vibration signals were collected using four accelerometers placed in vertical and horizontal directions at the coupling side and the opposite side of the system, allowing vibration responses to be observed from multiple orientations. For each accelerometer, 420 signals were recorded, with each signal consisting of 25,000 data points sampled at a frequency of 25 kHz (approximately one second duration). The data are organized such that each file has a structure of (4, 25,000), where rows represent sensor channels and columns represent sampled data. For this study, a subset of the dataset was selected, including Test 02 (misalignment), Test 04 (unbalance), and Test 06 (normal condition). All four sensor channels were analyzed separately to capture directional differences in vibration behavior. The shaft rotational speed during the tests was approximately 1238 rpm (20.63 Hz), which serves as a reference for identifying harmonic components in the vibration signals.

3.3 Signal Preprocessing & Analysis

All signals were prepared in MATLAB before analysis to keep both datasets consistent. The bearing dataset was already in MATLAB (.mat) format and could be used directly, while the belt-driven dataset was originally in NumPy (.npy) format and was converted to (.mat) using MATLAB with Python integration. This allowed all data to be processed in the same environment. For the Mendeley dataset, the data structure was checked before analysis. The dataset contains 420 vibration signals, where each signal includes data from four sensors, and each sensor records 25,000 data points. This can be

represented as (420 × 4 × 25,000). After separating the sensor channels, the data for each sensor becomes a matrix of size (420 × 25,000), which allows each sensor to be analyzed individually. These steps ensure consistency and reliability of the signals before analysis.

Since the dataset is large, it was not practical to compare all 420 signals at the same time. Therefore, one representative signal was selected for each case. To do this, the RMS value of each signal was calculated after removing its mean value, and the signal closest to the median RMS was chosen. This approach avoids selecting extreme signals and ensures a representative vibration behavior.

After selection, the signals were checked for length, orientation, and correct sensor assignment, and any incomplete or corrupted data were removed. In addition, the mean value of each signal was removed to eliminate DC offset and improve the accuracy of further analysis. These vibration features indicate the type of fault and the need for maintenance intervention before the condition becomes severe.

3.3.1 Time Domain Analysis

Time-domain analysis methods described in Chapter 2 were applied to observe how the vibration signals change over time. The selected representative signals from each condition were plotted in MATLAB using a time vector based on the sampling frequency, and the signals were compared by evaluating normal condition against unbalance and misalignment separately. In addition, each sensor channel was analyzed and compared individually to capture directional differences in vibration behavior. The analysis focused on identifying differences in amplitude, peak values, and overall waveform patterns between normal and faulty conditions. Statistical features such as RMS, peak value, crest factor, kurtosis, and variance were also calculated from the time-domain signals to describe the vibration behavior. These features provide information about signal energy, peak levels, and impulsive characteristics, which are useful for distinguishing between normal and faulty conditions. By combining signal plots and statistical features, differences in vibration behavior could be clearly identified before further analysis in the frequency domain.

3.3.2 Frequency Domain Analysis

Frequency-domain analysis methods described in Chapter 2 were performed to examine the frequency components of the vibration signals. The selected representative signals

from each condition were transformed from the time domain to the frequency domain using Fast Fourier Transform (FFT) in MATLAB. The analysis was carried out by comparing normal condition with unbalance and misalignment separately, and each sensor channel was analyzed individually to observe directional differences in frequency response. The frequency spectra were used to identify dominant frequency components, particularly the shaft rotational frequency (1X) and its harmonics (2X, 3X). The shaft frequency was calculated based on the rotational speed and used as a reference in the analysis. By comparing the amplitude and distribution of frequency components, differences between normal and faulty conditions could be clearly observed, allowing identification of fault-related characteristics in the vibration signals.

3.3.3 Envelope Analysis

Envelope analysis methods described in Chapter 2 were performed to detect high-frequency components related to bearing faults using the CWRU dataset. Since the dataset was already available in MATLAB (.mat) format, it was directly used for analysis without additional preprocessing steps.

The signals were processed in MATLAB to extract the envelope, allowing clearer observation of impulsive behavior caused by bearing defects. The analysis focused on comparing normal condition and bearing fault signals, while each sensor position was examined separately. By analyzing the envelope spectrum, characteristic fault frequencies could be identified more clearly, providing improved detection of bearing-related defects that are not always visible in standard time-domain or frequency-domain analysis.

3.4 Signal Tracking & Fault Identification

Under healthy operating conditions, an electric motor runs smoothly without mechanical faults such as unbalance, misalignment, or bearing damage, resulting in a stable vibration response. When a fault begins to develop, the motor can still operate, but its vibration behavior becomes abnormal. If these changes are not detected early, the vibration levels may increase over time and lead to serious damage or failure. Therefore, early fault detection is important to reduce maintenance costs and prevent unexpected breakdowns.

In this study, vibration analysis was used to detect such faults at an early stage. Signal tracking and fault identification were carried out by analyzing vibration signals in both

time and frequency domains and comparing normal condition with faulty conditions. For unbalance, a dominant peak at the shaft rotational frequency (1X) was used as an indicator. For misalignment, higher harmonics such as 2X and 3X were used to identify the fault. For bearing faults, characteristic frequencies such as BPFI, BPFO, BSF, and FTF were used as reference values, especially in the envelope spectrum.

Fault identification is based on comparing vibration responses under normal and faulty conditions. When clear changes such as increased amplitude, strong harmonic components, or impulsive behavior are present, the system is considered to operate under faulty conditions. These vibration features indicate the type of fault and indicate the need for maintenance intervention before the condition becomes severe.

Chapter 4 Result & Discussion

4.1 Bearing Fault & Normal Condition

This section compares the vibration behavior of the system under normal operating conditions and bearing fault conditions using time-domain, frequency-domain, and envelope analysis. The aim is to understand how the existence of a bearing defect affects the overall vibration response

4.1.1 Time Domain Analysis

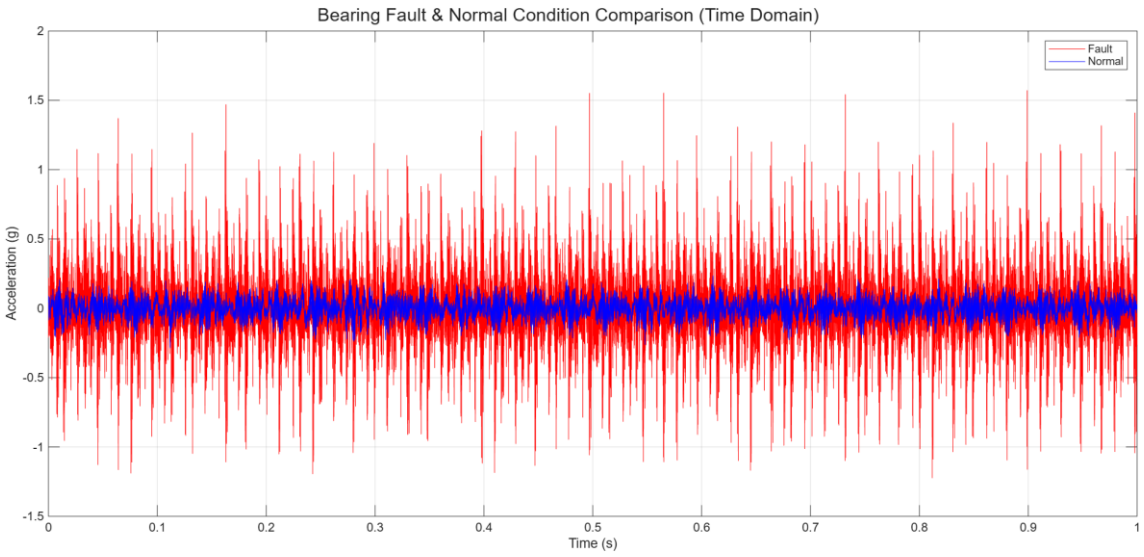


Figure 10 Time-domain comparison of normal and bearing fault conditions

Time-domain analysis was carried out to compare vibration signals under normal condition and bearing fault condition. As shown in *Figure 10*, the normal condition has a

stable signal with low amplitude and smooth waveform, while the bearing fault condition shows much higher amplitude and more irregular fluctuations. The fault signal clearly contains many sharp peaks, which indicate impulsive behavior caused by defects in the bearing.

Feature	Normal Condition	Bearing Fault	Difference (%)
RMS	0.0719	0.2912	305% ↑
Peak	0.2990	1.7256	480% ↑
Crest Factor	4.1583	5.9255	42% ↑
Kurtosis	2.7798	5.3959	94% ↑
Variance	0.0052	0.0848	1500% ↑

Table 1 Statistical feature comparison between normal and bearing fault conditions

The statistical features collectively confirm the presence of abnormal vibration behavior under the fault condition and reveal important characteristics of bearing damage. The large increase in RMS reflects a substantial rise in overall signal energy, which is consistent with the continuous generation of impact forces as rolling elements repeatedly contact the defective inner race surface. The disproportionately large increase in variance, relative to the more moderate increase in crest factor, indicates that the fault introduces high-energy random fluctuations distributed throughout the signal rather than a small number of extremely sharp, isolated spikes. The increase in kurtosis confirms that the signal distribution has heavier tails than under normal operation, which is consistent with the presence of periodic impulsive events. Taken together, these features indicate a fault condition with significant energetic disturbance, but they do not alone identify whether the fault originates from the inner race, outer race, or rolling elements. Frequency-domain and envelope analysis are therefore necessary to achieve fault localization.

Overall, both the waveform in *Figure 10* and the statistical results in *Table 1* clearly show that the bearing fault condition produces stronger, more irregular, and more impulsive vibrations compared to the normal condition. However, while time-domain analysis can clearly indicate abnormal behavior, it does not directly identify the exact fault location, which requires further analysis in the frequency domain and envelope spectrum.

4.1.2 Frequency Domain Analysis

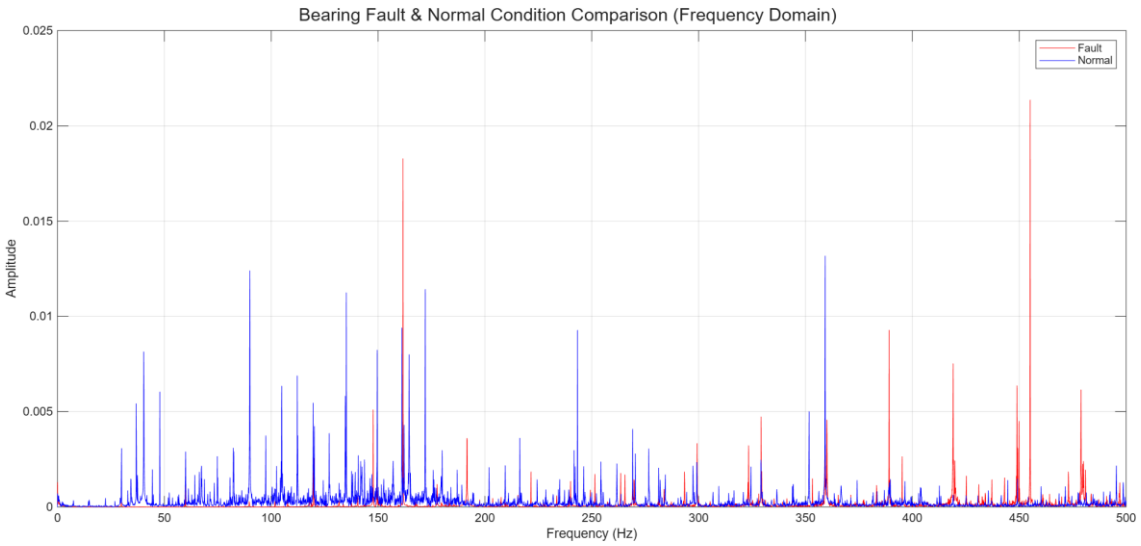


Figure 11 Frequency-domain (FFT) comparison of normal and bearing fault conditions

Frequency-domain analysis was carried out using FFT to understand how the vibration energy is distributed over different frequencies. As shown in *Figure 11*, the normal condition (blue) has low amplitude across the frequency range and does not show any strong peaks, which indicates stable operation. On the other hand, the bearing fault condition (red) shows higher amplitude and several noticeable peaks, especially at higher frequencies. These peaks are caused by additional vibration components generated by the bearing defect. Compared to the normal condition, the fault signal appears more complex and contains more frequency components.

However, even though these differences are visible, it is still difficult to clearly identify the exact fault type using only the FFT spectrum, because some frequency components overlap and the signal contains noise. Therefore, while frequency-domain analysis helps to detect abnormal behavior, it is not always enough to clearly identify bearing faults. For this reason, envelope analysis is used in the next section to better detect characteristic bearing fault frequencies.

4.1.3 Envelope Analysis

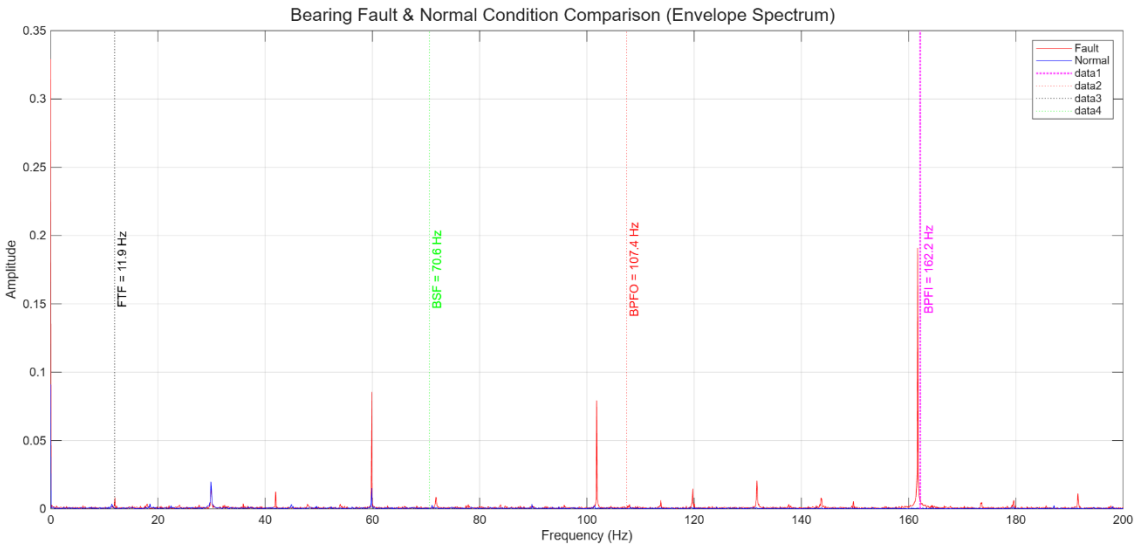


Figure 12 Envelope spectrum showing characteristic bearing fault frequencies

Envelope analysis was used to clearly detect the bearing fault. As shown in *Figure 12*, the normal condition (blue) has very low amplitude and does not show any clear peaks at the characteristic frequencies. On the other hand, the bearing fault condition (red) shows strong and clear peaks at specific frequencies. The most noticeable peak appears near the inner race fault frequency (BPFI), which indicates the presence of an inner race defect. These peaks are caused by repeated impacts when the rolling elements pass over the damaged part of the bearing.

The absence of clearly identifiable peaks at BPFO, BSF, and FTF in the envelope spectrum further supports this conclusion, as these frequencies correspond to outer race damage, rolling element damage, and cage defects respectively none of which were introduced in this dataset. The dominant BPFI peak therefore serves as a specific and unambiguous indicator of a localized inner race defect. Compared to the time-domain and frequency-domain results, the envelope spectrum makes the fault much easier to see and understand. This shows that envelope analysis is a very effective method for detecting bearing faults, especially at an early stage when the fault may not be clearly visible using other methods.

4.1.4 Discussion

The comparison between normal and bearing fault conditions clearly shows that the presence of a defect significantly changes the vibration behavior of the system. In the time domain, the fault condition produces a more irregular signal with strong impulsive peaks, which is supported by the large increases in RMS, kurtosis, and variance, indicating higher vibration energy and stronger impact events. In the frequency domain, the fault signal becomes more complex with higher amplitudes across a wide range of frequencies, but it remains difficult to clearly identify the exact fault due to overlapping components and noise. By applying signal tracking, the analysis focuses on key vibration features rather than the entire spectrum, making interpretation more reliable. In this case, tracking the envelope spectrum reveals a clear and dominant peak at the BPFI, which confirms the presence of an inner race defect. This indicates that the vibration is mainly caused by repeated impacts as rolling elements pass over the damaged area. Overall, while time-domain and frequency-domain analyses are useful for detecting abnormal behavior, signal tracking through envelope analysis provides a clearer and more accurate identification of the bearing fault.

4.2 Unbalance & Normal Condition

This section looks at how an unbalanced shaft creates vibration and how it differs from normal operation. In a normal condition, the shaft rotates smoothly because the mass is evenly distributed, so the vibration is relatively stable and low. When unbalance occurs, part of the mass is not evenly distributed, which creates a centrifugal force during rotation. This force acts once in every rotation and produces a repeating vibration pattern. In this study, the goal is not only to compare normal and unbalance conditions, but also to understand how to analyze and recognize unbalance using the Mendeley dataset. The analysis focuses on identifying key indicators of unbalance.

4.2.1 Time Domain & Frequency Domain Analysis

4.2.1.1 Sensor 1 Vertical Pulley side

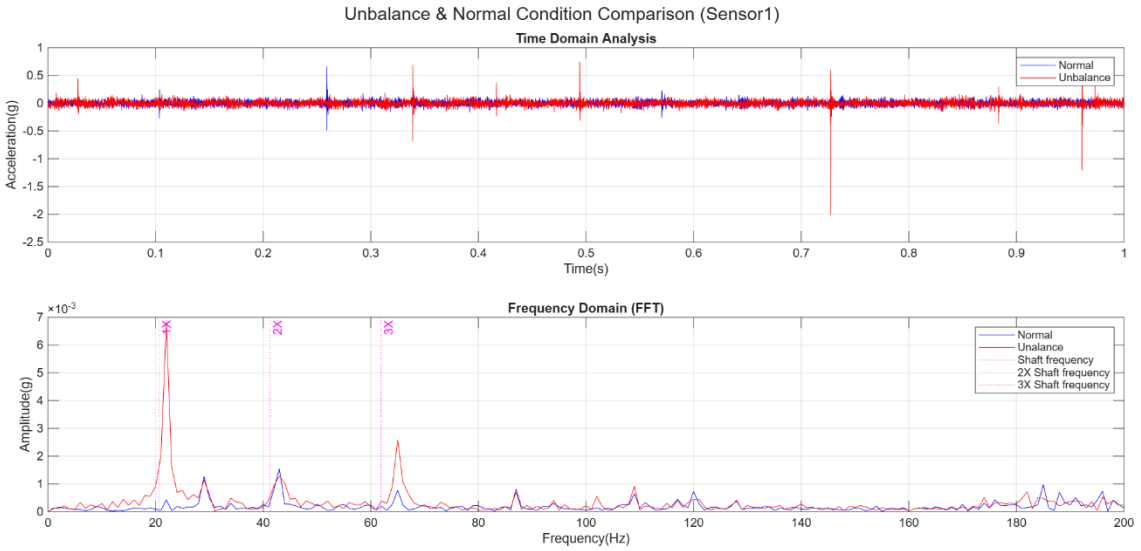


Figure 13 Time and frequency-domain comparison of normal and unbalance condition (Sensor 1)

Feature	Normal Condition	Unbalance	Differences (%)
RMS	0.0393	0.4869	1100% ↑
Peak	0.37514	1.43484	280% ↑
Crest Factor	9.429	28.766	205% ↑
Kurtosis	7.237	108.326	1300% ↑
Variance	1.5257e-03	2.3838e-03	56% ↑

Table 2 Statistical feature comparison between normal and unbalance condition for Sensor 1

Sensor 1 is positioned vertically on the side of the driven pulley, which makes it sensitive to radial vibration caused by shaft rotation. As shown in *Figure 13*, the time-domain signal for the normal condition (blue) is relatively stable with low amplitude, while the unbalance condition (red) shows higher amplitude and more noticeable variations, with slightly more irregular peaks. In the frequency-domain, the difference becomes clearer, where a strong peak appears at the shaft rotational frequency (1X) in the unbalance condition, which is the main indicator of unbalance, smaller harmonic peaks at 2X and 3X are also present but are considerably less dominant than the 1X component. For a theoretically pure unbalance condition, only the 1X component is expected. The presence of weak higher harmonics in this case is attributed to the nonlinear force transmission characteristics of

the belt-pulley system and minor structural asymmetries in the drivetrain, rather than to a secondary fault condition. This behavior is expected because the uneven mass creates a force that repeats once per rotation, and the vertical sensor near the driven pulley directly captures this radial effect.

The statistical features confirm a substantial increase in overall vibration energy under the unbalance condition, as reflected by the large increase in RMS. The peak value also increases considerably, indicating stronger amplitude excursions in the time-domain signal. It should be noted, however, that the very high kurtosis value observed under the unbalance condition is not directly attributable to the rotating unbalance itself. Unbalance generates a smooth sinusoidal force at the shaft frequency, which is not impulsive in nature and would not be expected to produce elevated kurtosis. The high kurtosis observed here is more likely associated with occasional transient events present in the signal, non-stationarities in the measurement, or existing minor irregularities in the system. The primary diagnostic indicator for unbalance remains the dominant 1X component in the frequency spectrum, not time-domain impulsiveness measures such as kurtosis.

4.2.1.2 Sensor 2 Horizontal Pulley side

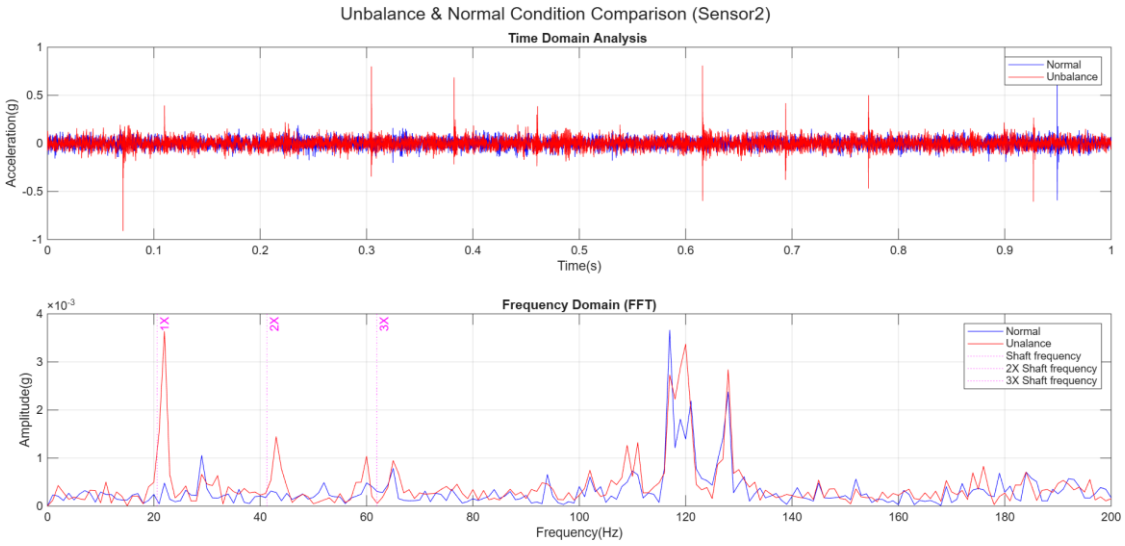


Figure 14 Time and frequency-domain comparison of normal and unbalance condition (Sensor 2)

Feature	Normal Condition	Unbalance	Differences (%)
RMS	0.04352	0.05227	20% ↑
Peak	0.45491	1.35685	198% ↑
Crest Factor	10.222	25.712	152% ↑
Kurtosis	8.848	60.399	583% ↑
Variance	1.8976e-03	2.7449e-03	45% ↑

Table 3 Statistical feature comparison between normal and unbalance condition (Sensor 2)

Sensor 2 is placed in the horizontal direction on the side of the driven pulley in the belt-driven system, so its response is different from the vertical sensor. As shown in *Figure 14*, the time-domain signals for both normal and unbalance conditions look quite similar, with only a small increase in amplitude and a few irregular peaks in the unbalance case. This means that the effect of unbalance is not very clearly visible in the time-domain for this sensor.

In the frequency-domain, a peak at the shaft rotational frequency (1X) can still be seen in the unbalance condition, but it is weaker compared to Sensor 1. This is because the unbalance force acts in a radial direction and rotates with the shaft, while the horizontal sensor only captures part of this motion. At the same time, strong peaks appear in the **100** to **140** Hz range under both conditions, which are attributed to structural resonance, belt-pulley dynamics, and the lower lateral stiffness of the horizontal direction rather than to the fault itself. This resonance behavior also explains the apparent discrepancy between the large increase in peak value (198%) and the comparatively small increase in RMS (20%). Structural resonance can produce brief, high-amplitude bursts in the signal that drive the peak value upward without significantly contributing to overall signal energy, which is what RMS measures. The peak increase at this sensor therefore reflects resonance amplification rather than a strong unbalance response.

The statistical features show a similar trend, where the overall vibration level increases slightly, but peak-related and impulsive characteristics increase more noticeably. Overall, Sensor 2 can still detect unbalance through the 1X component, but the response is weaker and more influenced by system behavior, showing that sensor position and direction play an important role in vibration analysis.

4.2.1.3 Sensor 3 Vertical Disk side

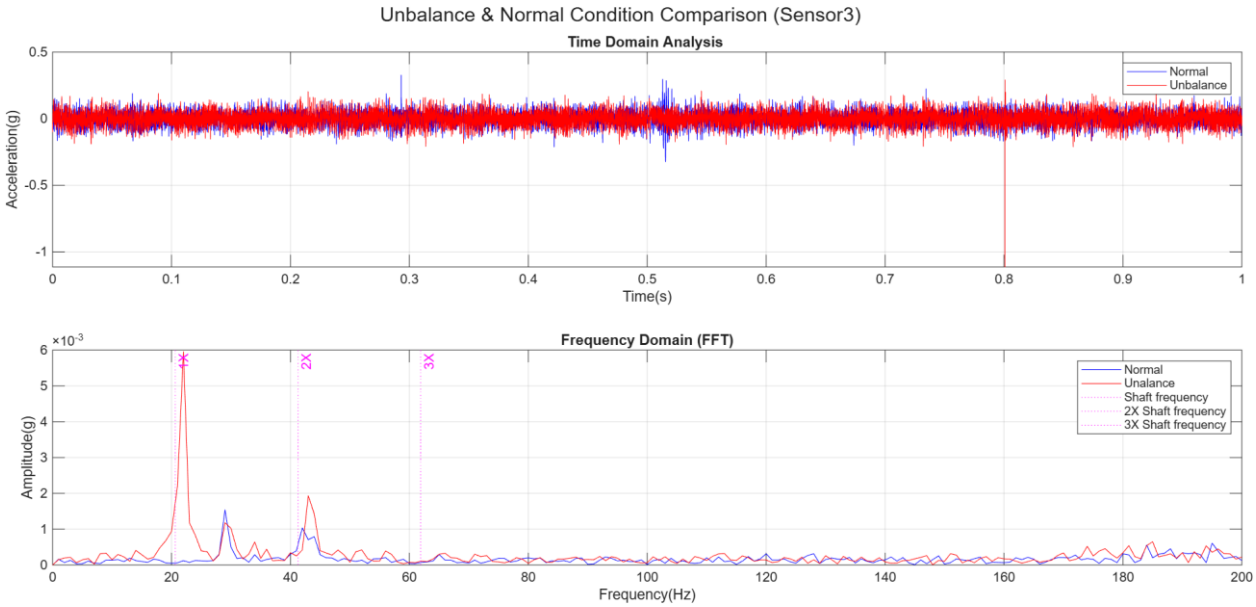


Figure 15 Time and frequency-domain comparison of normal and unbalance condition (Sensor 3)

Feature	Normal Condition	Unbalance (Sensor 3)	Differences (%)
RMS	0.04999	0.05232	4.7% ↑
Peak	0.27485	0.30767	12% ↑
Crest Factor	5.482	5.870	7% ↑
Kurtosis	3.165	3.252	2.7% ↑
Variance	2.5026e-03	2.7396e-03	9.5% ↑

Table 4 Statistical feature comparison between normal and unbalance condition for Sensor 3

Sensor 3 is placed vertical side of the coupling on the side of the disk. Although the unbalance is intentionally introduced at the rotating disk and, it does not show the highest vibration response. The statistical features increase only slightly, indicating that both the overall vibration energy and impulsive behavior remain nearly unchanged. This suggests that the fault effect is weak at this location.

In the frequency-domain, a peak at the shaft rotational frequency (1X) is still present under the unbalance condition, but the increase is small compared to other sensors. The harmonic components also do not show a strong difference. This confirms that although the fault exists, its influence is not strongly transmitted to this sensor.

This behavior shows that vibration is not only related to distance from the fault, but mainly depends on how forces are transmitted through the system. In the belt-driven system, the pulley side carries higher dynamic load, while the disk side is less excited. Therefore, Sensor 3 captures weaker fault-related vibration even though it is closer to the unbalance source.

4.2.1.4 Sensor 4 Horizontal Disk side

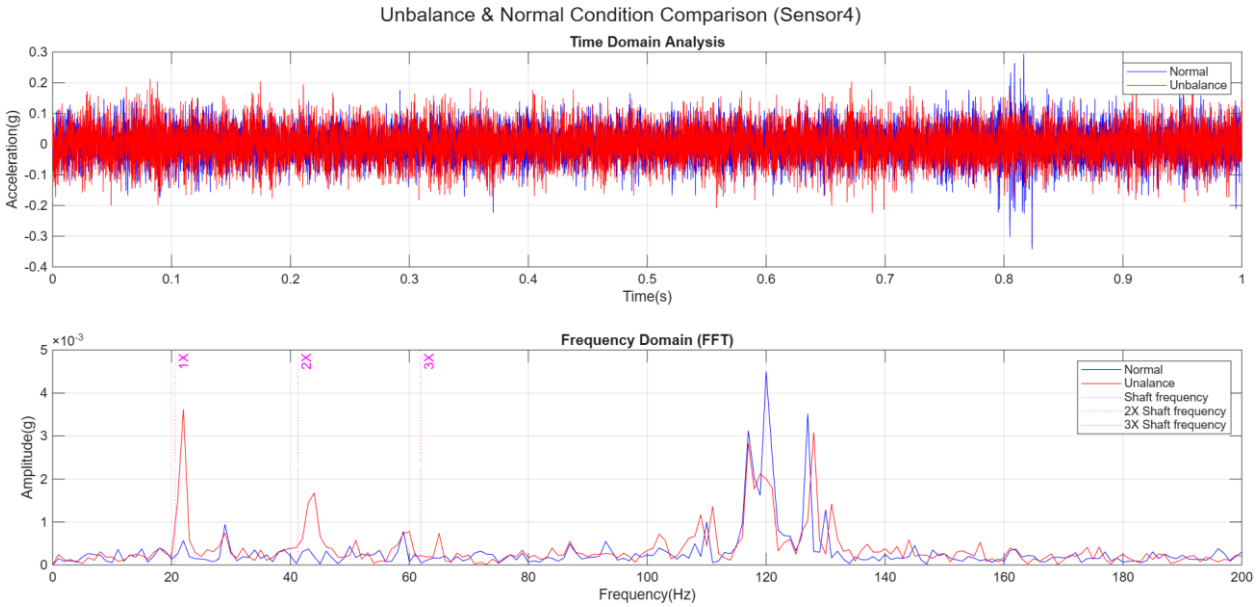


Figure 16 Time and frequency-domain comparison of normal and unbalance condition (Sensor 4)

Feature	Normal Condition	Unbalance (Sensor 4)	Differences (%)
RMS	0.04934	0.05318	7.8% ↑
Peak	0.25769	0.28890	12.1% ↑
Crest Factor	5.207	5.425	4.2% ↑
Kurtosis	3.169	3.202	1.0% ↑
Variance	2.4371e-03	2.8302e-03	16.1% ↑

Table 5 Statistical feature comparison between normal and unbalance condition for Sensor 4

Sensor 4 is located on the disk side of the shaft and measures vibration in the horizontal direction. Although it is closest to where the unbalance mass was added, it shows the weakest response among all sensors. In the time-domain, the normal and unbalance signals look almost identical, and in the frequency-domain, the 1X peak is very weak. Instead, the dominant peaks appear around 100–140 Hz in both conditions, indicating that they are caused by structural resonance rather than the fault. The

statistical features also show only small changes, with all values increasing slightly and kurtosis remaining close to 3, which suggests a normal, non-impulsive signal. This confirms that the unbalance has little effect at this sensor location.

This happens because vibration energy is not only related to distance from the fault but depends on how forces are transmitted through the system. In a belt-driven setup, the pulley side carries higher dynamic load due to belt tension, while the disk side receives less of this energy. As a result, Sensor 4 mainly captures structural vibration rather than the fault itself.

4.2.2 Discussion

Sensor Position and Direction: The results show that sensor position and direction have a strong effect on how unbalance is observed. Vertical sensors clearly capture the unbalance because they are aligned with the radial force of the rotating mass, resulting in higher amplitude and a strong 1X component. In contrast, horizontal sensors show lower amplitude at 1X but include additional high-frequency peaks (100–140 Hz), which are mainly caused by structural resonance and belt–pulley effects. It is also observed that sensors on the disk side show lower vibration energy compared to the pulley side, as the belt-drive system redistributes vibration energy, amplifying it near the pulley while reducing it on the disk side. From a signal tracking perspective, this behavior is confirmed by following the 1X component across different sensors, where it is strongest at the vertical pulley-side sensor and becomes weaker toward the disk side.

Statistical Features: The statistical features support these observations. RMS and variance increase under unbalance, showing higher vibration energy and instability. Peak and crest factor indicate stronger dynamic forces, while kurtosis highlights periodic high-amplitude behavior, especially near the pulley side. On the disk side, the changes are smaller, confirming that the fault effect is weaker there.

Statistical Features	Sensor 1	Sensor 2	Sensor 3	Sensor 4	Physical Meaning
RMS	1100% ↑	20% ↑	4.7% ↑	7.8% ↑	Overall signal energy level
Peak	280% ↑	198% ↑	12% ↑	12.1% ↑	Maximum dynamic amplitude
Crest Factor	205% ↑	152% ↑	7% ↑	4.2% ↑	Signal peak-to-energy ratio
Kurtosis	1300% ↑	583% ↑	2.7% ↑	1.0% ↑	Signal impulsiveness
Variance	56% ↑	45% ↑	9.5% ↑	16.1% ↑	Degree of signal fluctuation around the mean

Table 6 Summary of statistical feature changes for unbalance across all sensors

Effect on the Electric Motor: Even though the unbalance is introduced on the disk, its effect travels back to the motor through the shaft and belt. The rotating unbalanced mass creates a repeating load that forces the motor to work harder each cycle. Over time, this can increase bearing wear, vibration, and energy loss. The belt reduces part of the vibration, but it cannot fully eliminate the effect, so the motor still experiences continuous dynamic loading. Overall, unbalance can be identified by the 1X frequency and increased vibration levels, but correct interpretation depends on understanding sensor location and system behavior.

4.3 Misalignment & Normal Condition

This section examines how misalignment in a shaft system creates vibration and how it differs from normal operation. In a normal condition, the shafts are properly aligned, allowing smooth rotation and stable, low vibration. When misalignment occurs, the shafts are not in the same line, which introduces additional forces during rotation. Unlike unbalance, which mainly creates vibration once per rotation (1X), misalignment produces repeated mechanical interaction between components, resulting in vibration at multiple frequencies, especially **2X and 3X**.

In this study, the goal is not only to compare normal and misalignment conditions, but also to understand how to analyze and recognize misalignment using the Mendeley dataset. The analysis focuses on identifying key indicators of misalignment based on changes in vibration patterns across different sensors.

4.3.1 Time Domain & Frequency Domain Analysis

4.3.1.1 Sensor 1: Vertical Pulley side

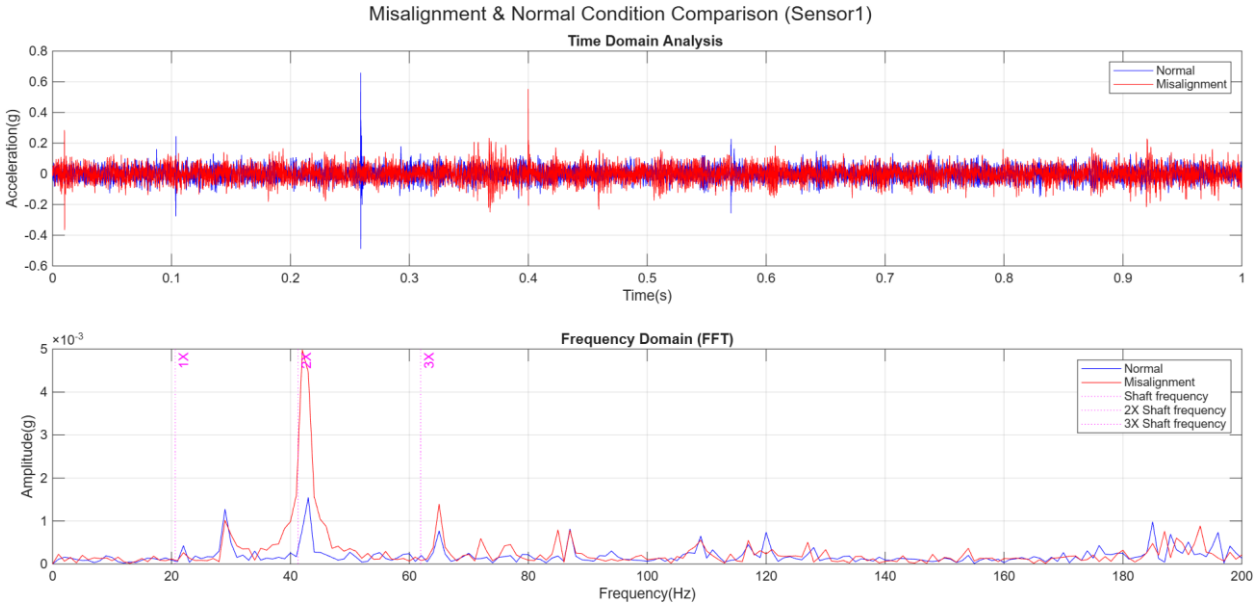


Figure 17 Time and frequency-domain comparison of normal and misalignment condition (Sensor 1)

Feature	Normal Condition	Misalignment (Sensor 1)	Differences (%)
RMS	0.03903	0.04713	20.8% ↑
Peak	0.37514	0.47013	25.3% ↑
Crest Factor	9.429	9.837	4.3% ↑
Kurtosis	7.237	7.406	2.3% ↑
Variance	1.5257e-03	2.2245e-03	45.8% ↑

Table 7 Statistical feature comparison between normal and misalignment condition for Sensor 1

Sensor 1 is placed in the vertical direction on the side of the driven pulley, where vibration effects are usually more noticeable. As shown in *Figure 17*, the time-domain signals for normal and misalignment conditions look similar overall, but the misalignment case shows a slightly higher amplitude and more variation in the signal. In the frequency-

domain, the difference is easier to see, where the 1X component is still present, but the peaks at **2X and 3X** become more visible under misalignment. These higher harmonics are typical indicators of misalignment and result from repeated mechanical interaction between components that are not properly aligned. The statistical features show a moderate increase in vibration, with RMS and peak values increasing to indicate higher overall vibration levels, while crest factor and kurtosis change only slightly, suggesting that the signal does not become more impulsive. The variance increases more clearly, indicating that the signal becomes less stable. Overall, Sensor 1 shows that misalignment leads to a moderate increase in vibration and introduces stronger harmonic components, especially at 2X and 3X, confirming that misalignment is more clearly identified in the frequency-domain than in the time-domain.

4.3.1.2 Sensor 2 Horizontal Pulley side

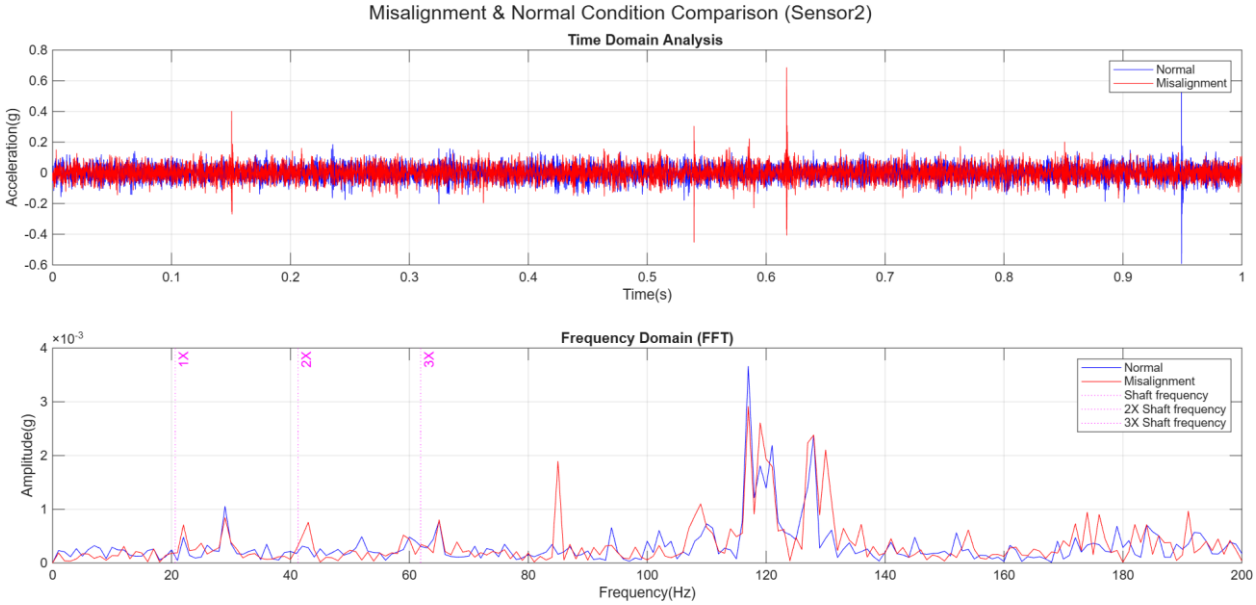


Figure 18 Time and frequency-domain comparison of normal and misalignment condition (Sensor 2)

Feature	Normal Condition	Misalignment (Sensor 2)	Differences (%)
RMS	0.04352	0.04604	5.8% ↑
Peak	0.45491	0.48656	7% ↑
Crest Factor	10.222	10.399	1.7% ↑
Kurtosis	8.848	7.955	10.1% ↓
Variance	1.8976e-03	2.1234e-03	11.9% ↑

Table 8 Statistical feature comparison between normal and misalignment condition for Sensor 2

In the frequency-domain, the vibration behavior under misalignment does not show a strong distinction from the normal condition. The peak at the shaft rotational frequency (1X) is present, but the harmonic component at **2X**, which is typically a key indicator of misalignment, does not show a clear increase and remains almost the same as in the normal condition. This suggests that the misalignment effect is not strongly captured by this sensor. At the same time, strong peaks are observed in the higher frequency range, around **100–140 Hz**, but these peaks appear in both normal and misalignment conditions. This indicates that they are not related to the fault, but are caused by **structural resonance** of the system. In a belt-driven setup, components such as the bearing housing and supporting structure have natural frequencies that can be excited during operation, especially in the horizontal direction where the system is less stiff. As a result, these structural vibrations dominate the spectrum and can mask the fault-related components.

The statistical features support this observation, showing only small changes in RMS, peak, and variance, which indicates a slight increase in vibration energy, while crest factor changes very little and kurtosis even decreases slightly, suggesting no increase in impulsive behavior. Overall, this confirms that the misalignment effect is weak in this sensor, and the horizontal direction is not sensitive to this type of fault. Instead, the measured signal is dominated by structural vibration, making it difficult to clearly identify misalignment from this sensor alone.

4.3.1.3 Sensor 3 Vertical Disk side

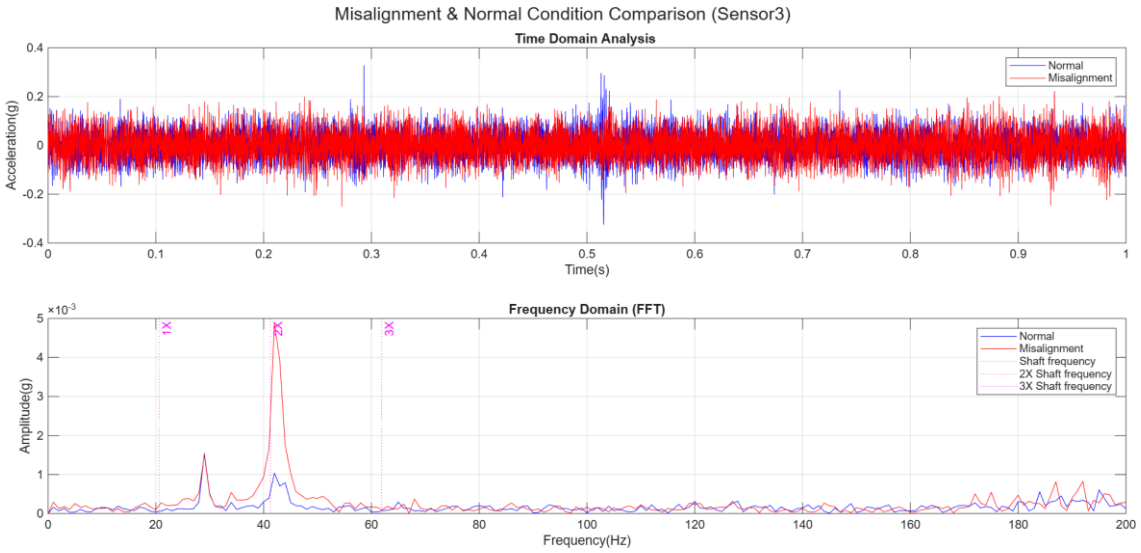


Figure 19 Time and frequency-domain comparison of normal and misalignment condition (Sensor 3)

Feature	Normal Condition	Misalignment (Sensor 3)	Differences (%)
RMS	0.04999	0.05513	10.3% ↑
Peak	0.27485	0.31597	15.0% ↑
Crest Factor	5.482	5.723	4.4% ↑
Kurtosis	3.165	3.342	5.6% ↑
Variance	2.5026e-03	3.04345e-03	21.6% ↑

Table 9 Statistical feature comparison between normal and misalignment condition for Sensor 3

Sensor 3 is placed in the vertical direction on the disk side, and it shows only a moderate response to the misalignment fault. In the time-domain, the signals for normal and misalignment conditions look very similar, with only a small increase in amplitude. In the frequency-domain, the 1X component is still present, and a slight increase can be seen at **2X**, but the difference is not as clear as in Sensor The statistical features follow the same trend. The RMS, peak, and variance increase moderately, which shows that the overall vibration level becomes higher. However, the crest factor and kurtosis change only slightly, meaning the signal does not become more impulsive.

Overall, Sensor 3 can detect misalignment, but the effect is not very strong. This is because the sensor is located on the disk side, where the dynamic loading is lower compared to the pulley side. As a result, part of the fault-related vibration is reduced

before reaching this location. This again shows that sensor position plays an important role in how clearly a fault can be detected.

4.3.1.4 Sensor 4

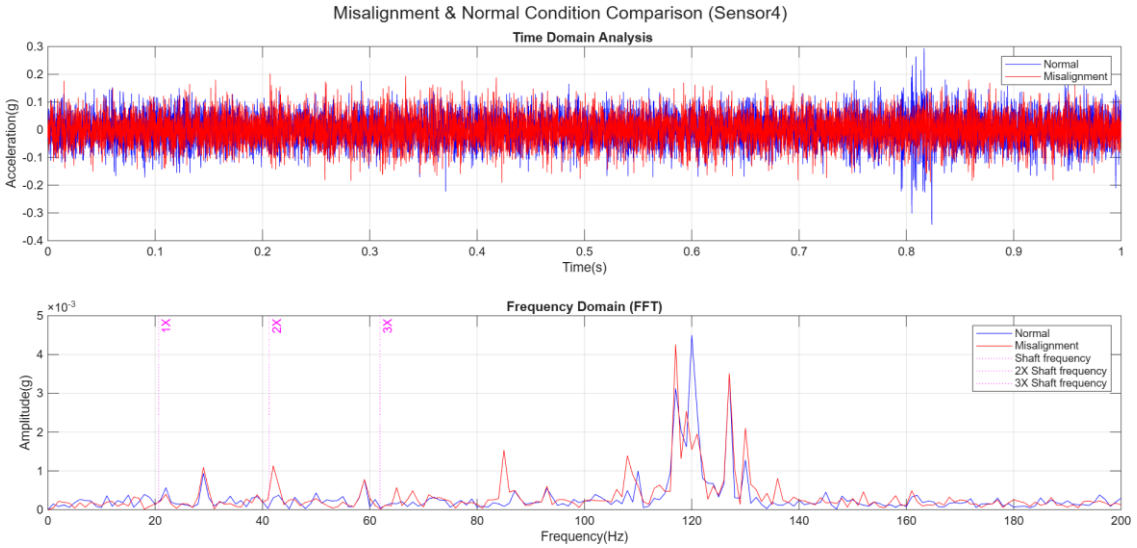


Figure 20 Time and frequency-domain comparison of normal and misalignment condition (Sensor 4)

Feature	Normal Condition	Misalignment (Sensor 4)	Differences (%)
RMS	0.04934	0.04856	1.6% ↓
Peak	0.25769	0.26961	4.6% ↑
Crest Factor	5.207	5.542	6.4% ↑
Kurtosis	3.169	3.305	4.3% ↑
Variance	2.4371e-03	2.3614e-03	3.1% ↓

Table 10 Statistical feature comparison between normal and misalignment condition for Sensor 4

Sensor 4 is placed in the horizontal direction on the disk side, and it shows the weakest response to the misalignment fault. In the time-domain, the signals for normal and misalignment conditions look almost the same, with no clear difference in amplitude or pattern. In the frequency-domain, the 1X component is visible, but the expected misalignment indicators at **2X and 3X** do not increase noticeably.

The statistical features also show very small and mixed changes. Some values increase slightly while others decrease, which means the overall vibration level stays almost the same. This confirms that the misalignment effect is very weak at this sensor location.

As seen in other sensors, strong peaks appear around **100–140 Hz** in both conditions, showing that these are caused by structural vibration, not the fault. At this position, the effect of belt tension is low, and the horizontal direction is mainly influenced by the structure itself. Because of this, the fault-related vibration is not clearly seen.

Overall, Sensor 4 is not suitable for detecting misalignment. This shows that even if a fault exists, it may not be visible at every sensor position, and choosing the right sensor location is very important in vibration analysis.

4.3.2 Discussion

Sensor Position and Direction: The results show that sensor position and measurement direction strongly influence how unbalance is observed. Vertical sensors capture the unbalance more clearly because they are aligned with the radial force of the rotating mass, resulting in higher vibration amplitude and a more visible 1X component. In contrast, horizontal sensors show a weaker response at 1X but capture additional peaks at higher frequencies (around 100–140 Hz), which are mainly related to structural resonance and belt–pulley effects rather than the fault itself. It is also observed that sensors on the disk side measure lower vibration levels compared to those on the pulley side, as the belt-drive system redistributes vibration energy, amplifying it near the pulley and reducing it toward the disk side. From a signal tracking perspective, this behavior is confirmed by following the 1X component across all sensors, where it is strongest at the vertical pulley-side sensor and gradually decreases toward the disk side.

Statistical Features: The statistical results support these observations. RMS and variance increase under unbalance, indicating higher vibration energy and greater variation in the signal, while peak and crest factor reflect stronger dynamic forces. Kurtosis shows changes in signal shape, particularly where higher peaks are present. These changes are more pronounced near the pulley side and smaller on the disk side, which is consistent with the variation of the tracked 1X component across sensor positions.

Statistical Features	Sensor 1	Sensor 2	Sensor 3	Sensor 4	Meaning
RMS	20.8% ↑	5.8% ↑	10.3% ↑	1.6% ↓	Overall signal energy level

Peak	25.3% ↑	7% ↑	15.0% ↑	4.6% ↑	Maximum dynamic amplitude
Crest Factor	4.3% ↑	1.7% ↑	4.4% ↑	6.4% ↑	Signal peak-to-energy ratio
Kurtosis	2.3% ↑	10.1% ↓	5.6% ↑	4.3% ↑	Signal impulsiveness
Variance	45.8% ↑	11.9% ↑	21.6% ↑	3.1% ↓	Degree of signal fluctuation around the mean

Table 11 Summary of statistical feature changes for misalignment across all sensors

Effect on the Electric Motor: Even though the unbalance is introduced at the disk, its effect propagates through the shaft and belt back to the motor. The rotating unbalanced mass creates a repeating force that increases the load on the motor during each rotation. Over time, this can lead to increased bearing wear, higher vibration levels, and reduced efficiency. Although the belt reduces part of the vibration energy, it cannot eliminate it completely, so the motor continues to experience cyclic dynamic loading. From a signal tracking point of view, this repeating load is represented by the persistent 1X component, which reflects how the fault influences the system over time. Overall, unbalance can be identified by the dominant 1X frequency and increased vibration levels, but accurate interpretation depends on understanding sensor location, system behavior, and how key vibration components are tracked across the system.

Chapter 5 Conclusion

5.1 Summary of Findings

This study investigated how vibration analysis can be used to detect mechanical faults in electric motor systems, focusing on bearing defects, shaft unbalance, and misalignment. The analysis was carried out using the CWRU and Mendeley datasets, applying time-domain, frequency-domain (FFT), and envelope analysis methods. The results showed that bearing faults are most clearly identified using envelope analysis, where a distinct peak at the BPFI confirms inner race damage. Unbalance was consistently recognized by a strong 1X frequency component, while misalignment appeared through 2X and 3X harmonics, although without large changes in overall amplitude. Overall, the results show that each fault has its own vibration signature, and

reliable detection requires combining different analysis methods rather than relying on a single one.

5.2 Key Insights

5.2.1 System Behavior

Mechanical systems, including electric motors and their connected components, exhibit natural frequencies that can be excited during operation, leading to resonance, which produces high-amplitude vibration peaks that are not directly related to mechanical faults. In this study, some high-frequency components observed in the vibration signals were attributed to structural resonance rather than actual damage. In addition, the belt-driven configuration significantly affects how vibration propagates through the system, as vibration traveling through components such as shafts, pulleys, and belts undergoes energy redistribution, where certain frequency components are amplified while others are attenuated before reaching the sensor. As a result, the measured vibration signal represents a combination of fault-related and system-induced effects rather than a direct reflection of the fault source. These findings highlight that accurate vibration analysis requires not only signal processing techniques but also a clear understanding of system dynamics, and it is therefore essential to distinguish between fault-induced vibration and system-induced phenomena such as resonance to avoid incorrect interpretation of results.

5.2.2 Sensor Placement

The results clearly show that sensor placement and measurement direction have a strong influence on fault detection. Vertical sensors captured unbalance and misalignment more clearly because they are aligned with the main radial forces, while horizontal sensors were more affected by structural and resonance-related vibrations. It was also observed that sensors near the pulley side measured stronger vibration compared to those on the disk side, which means vibration does not travel evenly through the system. This highlights that choosing the right sensor position and direction is essential for getting reliable results.

5.2.3 Practical Understanding

From a practical point of view, this study shows that electric motors should not be analyzed as isolated machines, but as part of a connected system. Components such as shafts, pulleys, belts, pumps, and fans all influence the overall behavior. For example,

unbalance in the rotating shaft introduces cyclic loading that is transmitted back to the motor, increasing mechanical stress over time. Although the belt reduces part of the vibration energy, it does not eliminate it entirely. This means that detecting faults in connected components early can help prevent motor damage. In this way, monitoring connected parts becomes an important part of predictive maintenance, helping to improve reliability and reduce unexpected failures.

5.3 Limitations & Future work

This study has several limitations. First, the analysis was based on publicly available datasets rather than real industrial measurements, which may not fully represent complex operating conditions. Second, the belt-driven system introduces vibration transmission effects that can obscure certain fault features, making interpretation more challenging.

Future work could focus on experimental validation using real machinery, where vibration data can be collected under controlled conditions. In addition, the use of multiple sensors and advanced signal processing techniques could improve fault detection accuracy. Machine learning approaches may also be explored to automate fault classification and enhance predictive maintenance strategies.

In conclusion, this study shows that vibration analysis is not only a method for detecting faults, but also a way to better understand how mechanical systems behave. Accurate diagnosis depends on combining signal analysis with system-level understanding and proper measurement techniques. By doing this, more reliable condition monitoring can be achieved, helping to improve equipment performance, reduce maintenance costs, and ensure safer operation.

Reference

[1] Electrical4U. Electric motor: construction, working and types [Internet]. [cited 2026 Apr 30]. Available from: https://www.electrical4u.com/electric-motor/

[2] Scheffer C, Girdhar P. Practical machinery vibration analysis and predictive maintenance. Oxford: Elsevier; 2004.

[3] ResearchGate. Rapid control prototyping and analysis of a fault diagnosis and amplifying algorithm for broken rotor bar induction motor drives [Internet]. [cited 2026 Apr 30]. Available from: https://www.researchgate.net/publication/388336011

[4] Wowk V. Machinery vibration: measurement and analysis. New York: McGraw-Hill; 1991.

[5] Mobley RK. An introduction to predictive maintenance. 2nd ed. Burlington: Butterworth-Heinemann; 2002.

[6] Randall RB. Vibration-based condition monitoring: industrial, aerospace and automotive applications. Chichester: John Wiley & Sons; 2011.

[7] Thomson WT. Theory of vibration with applications. 5th ed. Upper Saddle River: Prentice Hall; 1997.

[8] Salman W. Machinery vibration analysis: training manual and practical case studies. 2nd ed. VibSolutions; 2025.

[9] Mobius Institute. Rotor unbalance and vibration analysis illustration [Internet]. [cited 2026 Apr 30]. Available from: https://www.mobiusinstitute.com/

[10] Erbessd Instruments. Misalignment vibration analysis and diagnostic guide [Internet]. [cited 2026 Apr 30]. Available from: https://www.erbessd-instruments.com/

[11] SKF. Rolling bearings: bearing components and fault frequencies [Internet]. Gothenburg: SKF Group; [cited 2026 Apr 30]. Available from: https://www.skf.com/

[12] Case Western Reserve University. Bearing Data Center [Internet]. Cleveland (OH): Case Western Reserve University; [cited 2026 Apr 30]. Available from: https://engineering.case.edu/bearingdatacenter

[13] Brito LC, Susto GA, Brito JN, Duarte MAV. Rotating machinery fault dataset: unbalance, misalignment, looseness [Internet]. Mendeley Data; 2023 [cited 2026 Apr 30]. Available from: https://data.mendeley.com/

[14] Vibromera. Harmonics [Internet]. [cited 2026 Apr 30]. Available from: https://vibromera.eu/glossary/harmonics/

Appendixes

Appendix 1 Conversion

This section shows the MATLAB script used to convert .npy files into .mat format and extract Sensor 1 data. The same method was applied to all sensors by changing only the sensor index.

```
clc
clear
close all

inputfolder = 'C:\Matlab_Conversion\Test_06_NormalCondition';

np = py.importlib.import_module('numpy');
files = dir(fullfile(inputfolder, '*.npy'));
fprintf('Found %D files \n', length(files));

for k = 1:length(files)

    filename = fullfile(inputfolder, files(k).name);

    data_py = np.load(py.str(filename));
    data = double(data_py);

    if size(data,1) ~=4
        data = data'
    end

    if k==1
        sensor1_all = zeros(length(files), size(data,2));
        fprintf('Data size confirmed: %d x %d\n', size(data, 1), size(data, 2));
    end

    sensor1_all(k,:) = data(1,:);
end

size(sensor1_all)

save(fullfile(inputfolder, 'NormalCondition_Sensor1.mat'), 'sensor1_all')

disp('Sensor 1 extracted and merged successfully')
```

Published with MATLAB® R2026a

Appendix 2

This section includes a representative MATLAB script used to compare normal and faulty conditions (unbalance and misalignment). The same analysis process was used for all sensors and fault cases with minor changes.

Appendix 2.1 Misalignment & Normal Condition

```
load('C:\Users\Dell\OneDrive\Desktop\Vib_Data\Mendeley_data\Sensor1\NormalCondition_S
ensor1.mat');
```

```
normal = sensor1_all;

load('C:\Users\Dell\OneDrive\Desktop\Vib_Data\Mendeley_data\Sensor1\Misalignment_Sens
or1.mat');
mis = sensor1_all;

fs = 25000;
rpm = 1238;

for k_n = 1:size(normal,1)
    x_n = normal(k_n,:) - mean(normal(k_n,:));
    rms_n_all(k_n) = rms(x_n);
end

target_n = median(rms_n_all);
[~, idx_rep1] = min(abs(rms_n_all - target_n));

signal_n = normal(idx_rep1,:);
signal_n = signal_n - mean(signal_n);

N_n=length(signal_n);

for k_m = 1:size(mis,1)
    x_m = mis(k_m,:) - mean(mis(k_m,:));
    rms_m_all(k_m) = rms(x_m);
end

target_m = median(rms_m_all);
[~, idx_rep2] = min(abs(rms_m_all - target_m));

signal_m = mis(idx_rep2,:);
signal_m = signal_m - mean(signal_m);

N_m = length(signal_m);

t_n = (0:N_n-1)/fs;
t_m = (0:N_m-1)/fs;

figure
sgtitle('Misalignment & Normal Condition Comparison (Sensor1)')
subplot(2,1,1)
plot(t_n, signal_n, 'b')
hold on
plot(t_m, signal_m, 'r')
title('Time Domain Analysis ')
xlabel('Time(s)')
ylabel('Acceleration(g)')
legend('Normal','Misalignment')
grid on

Y_n = fft(signal_n);
f_n = (0:N_n/2-1)*(fs/N_n);
Y_nhalf = abs(Y_n(1:N_n/2))/N_n;

Y_m = fft(signal_m);
f_m = (0:N_m/2-1)*(fs/N_m);
Y_mhalf = abs(Y_m(1:N_m/2))/N_m;

f_1x = rpm / 60;

fprintf('\n 1X = %.2f Hz\n', f_1x);
subplot(2,1,2)
plot(f_n, Y_nhalf, 'b')
hold on
plot(f_m, Y_mhalf, 'r')
xlim([0 200])
```

```
title('Frequency Domain (FFT)')
xlabel('Frequency(Hz)')
ylabel('Amplitude(g)')
legend('Normal','Misalignment')
xline(f_1x, 'm:','1X','DisplayName','Shaft frequency')
xline(2*f_1x, 'm:', '2X', 'DisplayName','2X Shaft frequency')
xline(3*f_1x, 'm:', '3X', 'DisplayName','3X Shaft frequency')
grid on

for k = 1:size(normal,1)
    x = normal(k,:) - mean(normal(k,:));
    rms_n_all(k)   = rms(x);
    peak_n_all(k)  = max(abs(x));
    crest_n_all(k) = peak_n_all(k)/rms_n_all(k);
    kurt_n_all(k)  = kurtosis(x);
    var_n_all(k)   = var(x);
end

for k = 1:size(mis,1)
    x = mis(k,:) - mean(mis(k, :));
    rms_m_all(k)   = rms(x);
    peak_m_all(k)  = max(abs(x));
    crest_m_all(k) = peak_m_all(k)/rms_m_all(k);
    kurt_m_all(k)  = kurtosis(x);
    var_m_all(k)   = var(x);
end

rms_n = mean(rms_n_all);
peak_n = mean(peak_n_all);
crest_n = mean(crest_n_all);
kurt_n = mean(kurt_n_all);
var_n = mean(var_n_all);

rms_m = mean(rms_m_all);
peak_m = mean(peak_m_all);
crest_m = mean(crest_m_all);
kurt_m = mean(kurt_m_all);
var_m = mean(var_m_all);
```

Published with MATLAB® R2026a

Appendix 2.2 Unbalance & Normal Condition

```
load('C:\Users\Dell\OneDrive\Desktop\Vib_Data\Mendeley_data\Sensor1\NormalCondition_S
ensor1.mat');
normal = sensor1_all;

load('C:\Users\Dell\OneDrive\Desktop\Vib_Data\Mendeley_data\Sensor1\Unbalance_Sensor1
.mat');
un = sensor1_all;

fs = 25000;
rpm = 1238;

for k_n = 1:size(normal,1)
    x_n = normal(k_n,:) - mean(normal(k_n,:));
    rms_n_all(k_n) = rms(x_n);
end

target_n = median(rms_n_all);
[~, idx_rep1] = min(abs(rms_n_all - target_n));

signal_n = normal(idx_rep1,:);
signal_n = signal_n - mean(signal_n);
```

```
N_n=length(signal_n);

for k_u = 1:size(un,1)
    x_u = un(k_u,:) - mean(un(k_u,:));
    rms_u_all(k_u) = rms(x_u);
end

target_u = median(rms_u_all);
[~, idx_rep2] = min(abs(rms_u_all - target_u));

signal_u = un(idx_rep2,:);
signal_u = signal_u - mean(signal_u);

N_u = length(signal_u);

t_n = (0:N_n-1)/fs;
t_u = (0:N_u-1)/fs;

figure
sgtitle('Unbalance & Normal Condition Comparison (Sensor1)')
subplot(2,1,1)
plot(t_n, signal_n, 'b')
hold on
plot(t_u, signal_u, 'r')
title('Time Domain Analysis')
xlabel('Time(s)')
ylabel('Acceleration(g)')
legend('Normal','Unbalance')
grid on

Y_n = fft(signal_n);
f_n = (0:N_n/2-1)*(fs/N_n);
Y_nhalf = abs(Y_n(1:N_n/2))/N_n;

Y_u = fft(signal_u);
f_u = (0:N_u/2-1)*(fs/N_u);
Y_uhalf = abs(Y_u(1:N_u/2))/N_u;

f_1x = rpm / 60;

fprintf('\n 1X = %.2f Hz\n', f_1x);
subplot(2,1,2)
plot(f_n, Y_nhalf, 'b')
hold on
plot(f_u, Y_uhalf, 'r')
xlim([0 200])
title('Frequency Domain (FFT)')
xlabel('Frequency(Hz)')
ylabel('Amplitude(g)')
legend('Normal','Unalance')
xline(f_1x, 'm:','1X','DisplayName','Shaft frequency')
xline(2*f_1x, 'm:', '2X', 'DisplayName','2X Shaft frequency')
xline(3*f_1x, 'm:', '3X', 'DisplayName','3X Shaft frequency')
grid on

for k = 1:size(normal,1)
    x = normal(k,:) - mean(normal(k,:));
    rms_n_all(k)   = rms(x);
    peak_n_all(k)  = max(abs(x));
    crest_n_all(k) = peak_n_all(k)/rms_n_all(k);
    kurt_n_all(k)  = kurtosis(x);
    var_n_all(k)   = var(x);
end

for k = 1:size(un,1)
```

```
    x = un(k,:) - mean(un(k, :));
    rms_u_all(k)   = rms(x);
    peak_u_all(k)  = max(abs(x));
    crest_u_all(k) = peak_u_all(k)/rms_u_all(k);
    kurt_u_all(k)  = kurtosis(x);
    var_u_all(k)   = var(x);
end
rms_n = mean(rms_n_all);
peak_n = mean(peak_n_all);
crest_n = mean(crest_n_all);
kurt_n = mean(kurt_n_all);
var_n = mean(var_n_all);

rms_u = mean(rms_u_all);
peak_u = mean(peak_u_all);
crest_u = mean(crest_u_all);
kurt_u = mean(kurt_u_all);
var_u = mean(var_u_all);

fprintf('\n===== COMPARISON =====\n')
fprintf('Feature         Normal        Unbalance\n')
fprintf('-------------------------------------------\n')
fprintf('RMS             %.5f       %.5f\n', rms_n, rms_u)
fprintf('Peak            %.5f       %.5f\n', peak_n, peak_u)
fprintf('Crest Factor    %.3f        %.3f\n', crest_n, crest_u)
fprintf('Kurtosis        %.3f       %.3f\n', kurt_n, kurt_u)
fprintf('Variance        %.6e  %.6e\n', var_n, var_u)
```

Published with MATLAB® R2026a

Appendix 3 Bearing Fault & Normal Condition

This section presents the MATLAB script used for comparing normal and bearing fault conditions. The same approach was applied throughout the analysis, with only small modifications depending on the dataset.

```
clear
clc
close all

load('Normal_0.mat')
x_normal = X097_DE_time;

load('Bearing_Fault_0.mat')
x_fault = X105_DE_time;

fs = 12000;
rpm = 1797;
f_shaft = rpm / 60;

N = min(length(x_normal), length(x_fault));

x_normal = x_normal(1:N);
x_fault  = x_fault(1:N);

x_normal = x_normal - mean(x_normal);
x_fault  = x_fault  - mean(x_fault);

t = (0:N-1)/fs;
BPFI = 5.4152 * f_shaft; %Ball Pass Frequency Inner Race
```

```
BPFO = 3.5848 * f_shaft; %Ball Pass Frequency Outer Race
FTF = 0.39828 * f_shaft; %Cage Train
BSF = 2.3576 * f_shaft; %Rolling Element

label_BPFI = sprintf('BPFI = %.1f Hz', BPFI);
label_BPFO = sprintf('BPFO = %.1f Hz', BPFO);
label_FTF  = sprintf('FTF = %.1f Hz', FTF);
label_BSF  = sprintf('BSF = %.1f Hz', BSF);

figure
sgtitle('Bearing Fault & Normal Condition Comparison (CWRU)')
subplot(3,1,1)
plot(t, x_fault, 'r')
hold on
plot(t, x_normal, 'b')
xlim([0 1])
title('Time Domain Comparison')
xlabel('Time (s)')
ylabel('Acceleration (g)')
legend('Fault','Normal')
grid on

Xn = fft(x_normal);
Xf = fft(x_fault);

P2n = abs(Xn)/N;
P2f = abs(Xf)/N;

P1n = P2n(1:floor(N/2)+1);
P1f = P2f(1:floor(N/2)+1);

P1n(2:end-1) = 2*P1n(2:end-1);
P1f(2:end-1) = 2*P1f(2:end-1);

f = fs*(0:floor(N/2))/N;

subplot(3,1,2)
plot(f, P1f, 'r')
hold on
plot(f, P1n, 'b')
xlim([0 500])
title('FFT Comparison')
xlabel('Frequency (Hz)')
ylabel('Amplitude')
legend('Fault','Normal');
xline(f_shaft,'m:','1X','DisplayName','Shaft Rotational Frequency')
xline(f_shaft*2,'m:','2X','DisplayName','2*Shaft Rotational Frequency')
xline(f_shaft*3,'m:','3X','DisplayName','3*Shaft Rotational Frequency')
grid on

env_n = abs(hilbert(x_normal));
env_f = abs(hilbert(x_fault));

En = fft(env_n);
Ef = fft(env_f);

EnvP1n = abs(En)/N;
EnvP1f = abs(Ef)/N;

EnvP1n = EnvP1n(1:floor(N/2)+1);
EnvP1f = EnvP1f(1:floor(N/2)+1);

EnvP1n(2:end-1) = 2*EnvP1n(2:end-1);
EnvP1f(2:end-1) = 2*EnvP1f(2:end-1);

subplot(3,1,3)
```

```
plot(f, EnvP1f, 'r')
hold on
plot(f, EnvP1n, 'b')
xlim([0 200])
title('Envelope Spectrum Comparison (Bearing Fault Detection)')
xlabel('Frequency (Hz)')
ylabel('Amplitude')
legend('Fault','Normal');
grid on

xline(BPFI, 'm:', label_BPFI, ...
    'LabelVerticalAlignment','middle', ...
    'LineWidth',1.5);

xline(BPFO, 'r:', label_BPFO, ...
    'LabelVerticalAlignment','middle');

xline(FTF, 'k:', label_FTF, ...
    'LabelVerticalAlignment','middle');

xline(BSF, 'g:', label_BSF, ...
    'LabelVerticalAlignment','middle');

RMS_n = rms(x_normal);
RMS_f = rms(x_fault);

Peak_n = max(abs(x_normal));
Peak_f = max(abs(x_fault));

Crest_n = Peak_n / RMS_n;
Crest_f = Peak_f / RMS_f;

Kurt_n = kurtosis(x_normal);
Kurt_f = kurtosis(x_fault);

Variance_n = var(x_normal);
Variance_f = var(x_fault);

fprintf('\n===== COMPARISON =====\n')
fprintf('Feature        Healthy      Fault\n')
fprintf('RMS            %.4f      %.4f\n', RMS_n, RMS_f)
fprintf('Peak           %.4f      %.4f\n', Peak_n, Peak_f)
fprintf('Crest Factor   %.4f      %.4f\n', Crest_n, Crest_f)
fprintf('Kurtosis       %.4f      %.4f\n', Kurt_n, Kurt_f)
fprintf('Variance       %.4f      %.4f\n', Variance_n, Variance_f)
```

Published with MATLAB® R2026a